Review Article

A General Review on Longwall Mining-Induced Fractures in Near-Face Regions

Qingsheng Bai [iD][1,2,3] **and Shihao Tu** [iD][1]

[1]*Key Laboratory of Deep Coal Resource Mining (CUMT), Ministry of Education of China, School of Mines, China University of Mining and Technology, Xuzhou 221116, China*
[2]*State Key Laboratory of Coal Resources and Safe Mining, China University of Mining and Technology, Xuzhou 221116, China*
[3]*University of Toronto, Department of Civil and Mineral Engineering, 170 College Street, Toronto, Canada M5S 3E3*

Correspondence should be addressed to Qingsheng Bai; qingsheng_bai@yahoo.com and Shihao Tu; tsh@cumt.edu.cn

It is believed that underground longwall mining usually produces fractures in the surrounding rocks. On the one hand, mining-induced fractures not only degrade the strength of the rock mass but also serve as main channels for fluids (e.g., water and methane). Fractures facilitate the failure of the rock mass and fluid inrush into working spaces. Therefore, mining-induced fractures are significant for the safety evaluation of underground structures and finding feasible solutions. On the other hand, the fractures are also beneficial for methane collection and coal fragmentation, which are essential for the successful operation of longwall top coal caving mining. Therefore, determining the characteristics of induced fractures is significant for underground longwall mining. From a global perspective, longwall mining-induced fractures in the overburden have been well studied, which improves the understanding of the mining pressure and ground control. However, induced fractures near the longwall face, which have more significant effects on mining activities, have not been summarized. The goal of this review paper is to provide a general summary of the current achievements in characterizing mining-induced fractures in near-face regions. The characteristics of mining-induced fractures in the coal wall, chain pillar, immediate roofs and top coal, and floors are reviewed and summarized. Remarks are made on the current progress of, fundamental problems with, and developments in methodologies for characterizing mining-induced fractures using methods such as field observations, small-scale laboratory tests, physical modeling, and numerical modeling. Based on a comprehensive analysis, the advantages and disadvantages of each method are discussed, and the ideal conditions for applying each of these methods are also recommended.

1. Introduction

Longwall mining is the most common method of underground coal mining all over the world. During the retreating of the longwall face, the primary equilibrium state is disturbed and, as a result, the surrounding rocks are unavoidably broken or fractured. The induced fractures not only degrade the strength of the rock mass but also serve as main channels for fluids [1–5]. Therefore, understanding the characteristics of induced fractures is significant for mining safety. From a global perspective, it is widely believed that three different disturbed zones are produced in the roof after

the extraction of a coal seam [6, 7]: the caved zone, fractured zone, and deformation zone (or subsidence/bending zone), as shown in Figure 1. Fractures also occur in the underlying strata. In general, the scope of the induced fractures in the roof is much larger than that in the floor.

In general, the caved zone is highly fragmented with large porosity and high permeability. The characteristics of the caved zone impact many issues related to ventilation, methane, and water control [8, 9]. A fractured zone is located immediately above the caved zone. Field and laboratory observations [10–13] have shown that strata in this zone usually break into blocks by vertical and/or subvertical fractures.
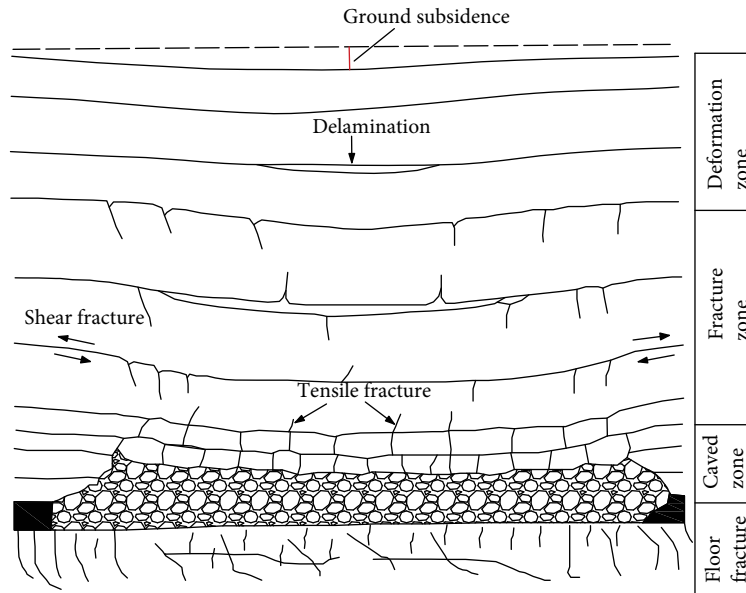
FIGURE 1: The global profile of longwall mining-induced fractures (modified from [6]).

The blocks do not move horizontally because of the lack of space, but they could move downward during the compaction of the caved zone. The fracture networks gradually decrease upward. Above the fractured zone is the continuous deformation zone, where the strata deform or bend without the development of major fractures. Empirical criteria predicting the extent of the caved and fractured zones have been developed in China with different lithological and geometric characteristics [14]. These empirical criteria are also employed in the American coal mining industry, but with some modifications [15, 16]. Factors affecting the disturbed zones such as in situ stress [17], physical properties of strata [18–21], inclination of the coal seam [7, 22], and surface topography [12, 23] have also been well studied.

Compared with induced fractures far away from the longwall panel, fractures close to the active longwall face usually develop rapidly because mining-induced stress is always concentrated in these locations. Figure 2 illustrates an idealized distribution of induced stress surrounding a longwall panel [6]. The front and side abutment stresses increase to a peak value at a distance from the longwall face into the solid seam and decrease with increasing distance and return to the virgin stress. It clearly shows that high stress is located near the workspaces (e.g., longwall face, head gateroads, and tail gateroads); therefore, fractures and failure usually develop quickly in these regions. Significant attention has been paid to these regions by characterizing the stress distribution, fracture development, and associated rock mass behavior.

Fractures in front of the longwall face are significant for the safety of the longwall face and dominate the seepage characteristics of methane in the coal seam. Fractures in the chain pillar determine the behavior of the pillar, which is an important part that maintains the stability of the gateroads. Fractures in the immediate roofs are an indicator of roof stability and are a primary index for roof control. In longwall top coal caving (LTCC), fractures in the top coal are the most significant factors to consider when assessing top coal cavability. Fractures in the floor have an adverse impact on longwall mining practice and play a significant role in safe mining above confined aquifers.

The objective of this paper is to review the effects of mining-induced fractures in near longwall face regions, including the longwall face, chain pillar, immediate roofs, top coal, and floors. This paper is organized as follows. The characteristics of induced fractures in these regions are outlined in Sections 2 to 5. For each near-face region, the most important characteristics of mining-induced fractures are illustrated. In Section 6, unresolved issues in characterizing mining-induced fractures by field observations, small-scale laboratory tests, physical modeling, and numerical modeling are presented in detail. Their capabilities and limitations are also discussed. At the end of this section, a comparative analysis is conducted between these study methods. For each method, the advantages or disadvantages are discussed, and ideal situations for applying each method are also suggested. Finally, concluding remarks are presented in Section 7. Understanding fracture characteristics is essential to evaluate the stability of the rock mass surrounding the active longwall face and to find feasible reinforcements for the damaged rock mass. As the main flow channels for fluids (e.g., water and methane), the fracture distributions determine the transport properties of these fluids. The summary presented in this paper can also be employed as a guide in developing strategies for methane collection and solutions to water inrush. As the primary index for top coal cavability, the fracture characteristics of top coal are also useful for cavability evaluation and identifying potential methods for increasing the recovery ratio of top coal. It should be noted that this review focuses on mining-induced fractures in near-face regions and is not exhaustive. For more extensive descriptions of longwall mining-induced fractures, the reader is referred to the textbooks [6, 7, 24, 25]. Field fracture observations using different methods can be found in [26–29]. For physical modeling of mining-related rock fractures, the
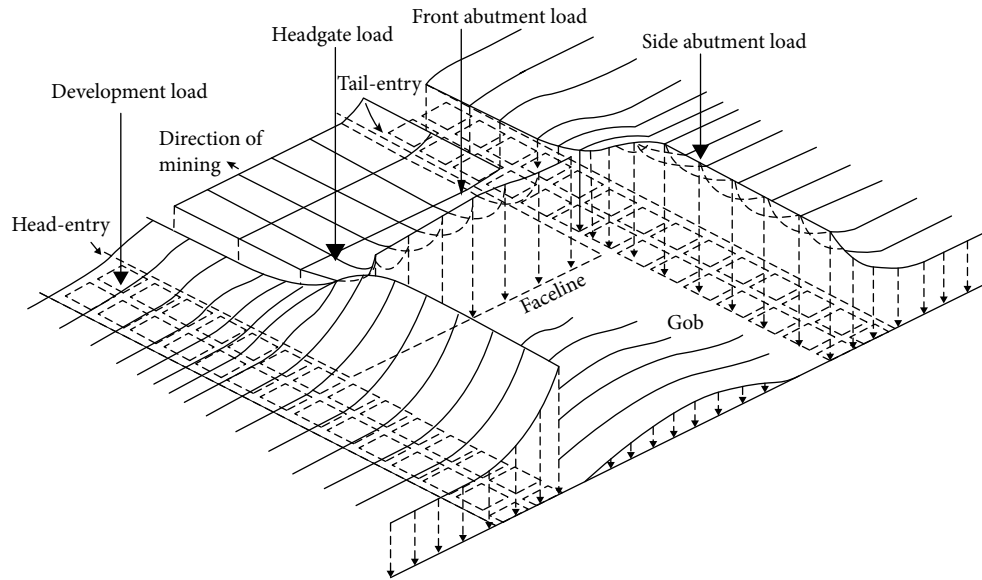
FIGURE 2: The schematic layout of the stress redistribution around a longwall mining panel [6].

reader is referred to [30–32]. For numerical simulations on rock fracturing, the reader can refer to [33–37] for details on the fundamentals and applications of the discrete element method (DEM).

2. Fractures in the Longwall Face

Fractures in the longwall face may cause face instability or spallings. Serious face spalling is one of the major threats to the safety of longwall mining [38–43]. The spalling of the face may also result in roof falls. The interaction between face spalling and roof fall not only disrupts the mining process but also causes equipment damage and even casualties in severe cases [44, 45]. Therefore, characterizing induced fractures in the longwall face is important for the safety evaluation of mining activities. This issue is attracting more and more attention as the cutting height in Chinese coal mines increases, which often produces serious longwall face spallings [46].

Researchers frequently determine the fracture scope (or failure zone) in front of the longwall face according to the distribution of the induced stress. According to the mechanical theory of elastoplastic behavior [47], the location of the peak stress of the front abutment loading can be regarded as the scope of the failure zone. Wilson [47] proposed a "stress balance" method to calculate the stress distribution in front of a longwall face. In the model, the yielded zone (or fractured zone) is determined by mining height, stress state, coal strength, and the supporting intensity applied to the face. Many field measurements have been conducted to understand the development of mining-induced stress in front of the longwall face [2, 48]. However, the stress distribution only indicates the fracture scope indirectly. Little information can be obtained on the distribution and development of the fractures.

Bai et al. [44] identified two types of face spallings in the brittle coal seam, which correspond to two different fracture characteristics. Tensile splitting failure was found in small areas near the face in the early stage after the face was exposed, which usually produces many small laminae spices, as shown in Figure 3(a). The tensile splitting failure indicates axial cracks (or fractures) parallel to the longwall face. In general, the laminae had thickness less than 0.3 m and sizes ranging from 0.1 to 0.8 m. Splitting first occurred in the middle of the face immediately after the shearer passed and then extended in both the vertical and horizon directions. The failure width reached its maximum in the middle level of the face, as shown in Figure 3(a). Field observations showed that the depth of the tensile splitting spalling is generally less than 0.6 m.

The shear slipping failure will follow the tensile splitting failure if the former does not cause large spalls. Shear slipping failure produces larger spalling blocks, as shown in Figure 3(b). The spalling profile indicates that shear fractures developed in the longwall face. Based on the shear slipping failure, some researchers theoretically studied the spalling mechanism in both hard coal and soft coal seams [49, 50]. However, the theory cannot explain the fragmented shear failure of the longwall face, as shown in Figure 3(b).

Li et al. [51] showed that fractures began from the upper corner and developed into the face. The simulation results agreed with the observed shear slipping failure [44]. Wan [52] reported that crushed squeezing failure usually occurs in the soft coal seam. He pointed out that the induced compressive pressure applied to the longwall face and the mining height are the primary factors affecting spalling. Yao et al. [53] numerically investigated the effects of the coal seam dip angle on longwall face fracturing. Subvertical fractures are dominant in the horizontal coal seam, which causes an arc-shaped failure zone. In the up-dip coal face, fractures originated in the upper part and propagated at an incline into the face.

Preexisting weak planes in the coal seam play an important role in coal fracturing and the associated spalling types
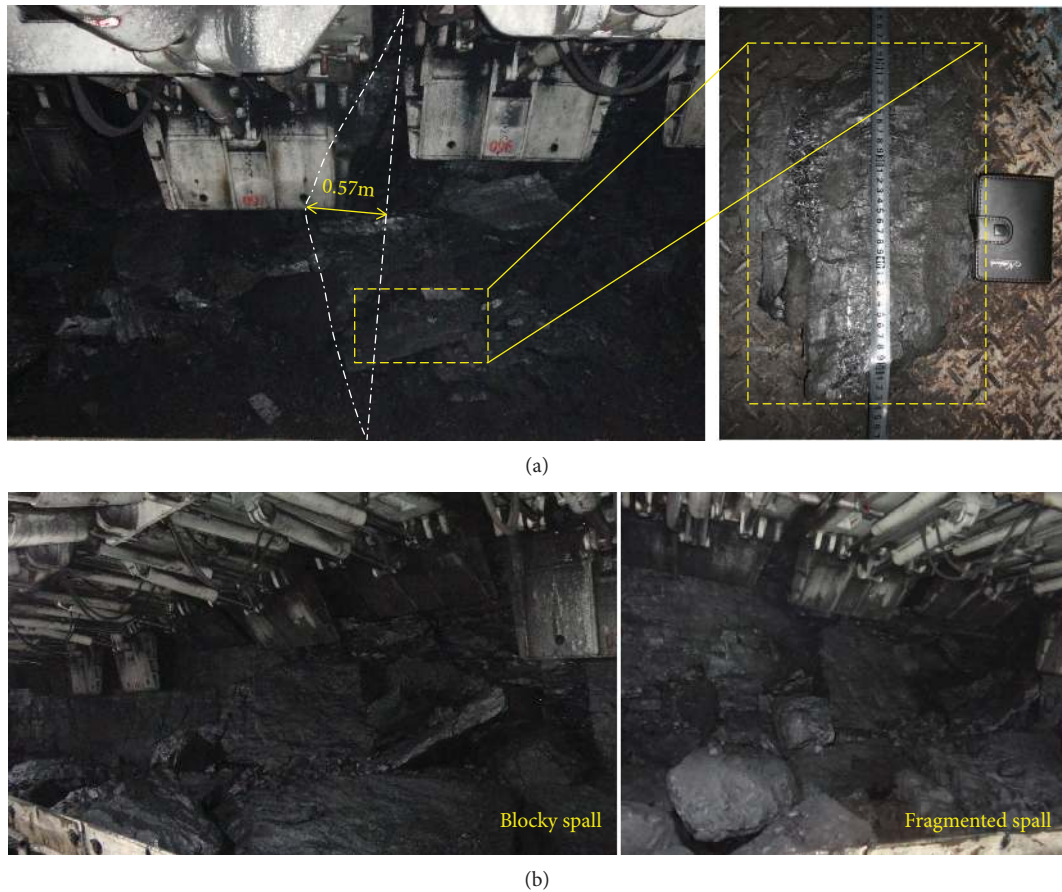
(a)

(b)

FIGURE 3: Observed tensile splitting failure (a) and shear slipping failure (b) in longwall face in a Chinese coal mine [44].

[38]. If only vertical weak planes are present in the coal seam, then fractures develop along these planes and lateral squeezing from the high induced stress may crush the slices, but this depends on the strength and thickness of the slices. If crisscross discontinuities are present in the coal, then fractures mainly propagate along the vertical planes, but lateral squeezing usually causes secondary fracturing along the horizontal planes, resulting in small fragments. In a case study, Yang et al. [54] developed a series of the DEM models to analyze the fracture characteristics impacted by weak planes. Their simulations showed that a series of conjugate planes dominated the fracturing of the face when bedding discontinuities were present in the coal seam. In jointed coal seams, the strength of the coal dominated the fracture profiles. In hard coal seams, the induced shear fractures conjugated to the opened discontinuities; in soft coal seams, parallel fractures were oriented toward the goaf.

3. Fractures in the Chain Pillar

Pillar strength is a significant part of underground coal mining. Over the past several decades, many pillar strength formulas have been developed for various coal fields around the world [55–57]. These strength formulas have been successfully used in the field; however, one obvious drawback is that they cannot provide information on pillar performance such as the strain behavior of the pillar during the mining process and how fractures develop in the pillar and their effect on pillar performance. Sometimes, these behaviors are also significant. For example, the chain pillar is not only designed to maintain the safety of the roadway but also serve as a barrier to prevent water and gas from migrating to the active face from the mined panels. Fractures in the pillar determine the transport properties of these fluids. Clearly, an understanding of progressive pillar fracturing (or failure) behavior in a complete mining environment is significant for pillar design.

Some field observations have shown that fracturing first occurs at the sides of pillar as slabbing or spalling and then propagates progressively into the center of the pillar. As a result, slender pillars typically generate an hourglass-shaped failure mode, which usually results from spalling near the pillar boundaries [58, 59]. Gradual shear fractures are usually observed after the spalling of a squat pillar [58]. Tensile fracture-induced spalling is a common failure mode of coal pillar under conditions in which weak floors or roofs exist or the interface between a pillar end and the surrounding rock is smooth and/or poorly bonded [24, 60, 61], as shown in Figure 4. The weak interface causes the pillar ends to slip when high loading is applied on the pillar. The interface failure weakens the horizontal resistance stress across the pillar ends and facilitates lateral straining of the pillar [24, 62]. Lateral moment near the pillar ends usually produces tensile fractures, and even blocky spallings when cleat and joint

(a)
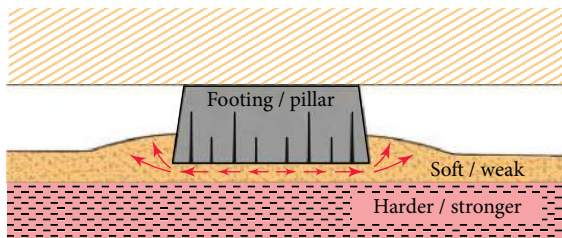
(b)

FIGURE 4: (a) Blocky rib spall along cleat planes due to weak interface lateral tension [24] and (b) pillar slabbing due to squeezing of the soft floor [24].

planes are ubiquitous within the coal seam, as shown in Figure 4(a). Advanced simulations showed that fractures propagate at a constant plunge and separation in the pillar with the frictionless interface. As the interface friction increases, fractures develop along ever more curved planes. At the same time, the distance between individual fractures decreases toward the core of the pillar [58, 59]. If the immediate roof or floor is much weaker than the coal seam, then they could fail in shear on the bedding planes or extrude laterally from the pillar ends. This causes the pillar undergo lateral tension, thus inducing tensile cracks that may extend from roof to floor and across the full width of the pillar [24, 61], as shown in Figure 4(b). Therefore, this type of fracture in the pillar is normally associated with floor heave [60].

Wilson [47] pointed out that there are two zones in the pillar which have totally different mechanical behavior. A yield zone adjacent to the boundary of the pillar will develop because the induced stress concentration generally exceeds the strength of the coal. The elastic core is surrounded by the yield zone. In China, there is a widely held belief that there are three distinct zones within a coal pillar [63]. A large
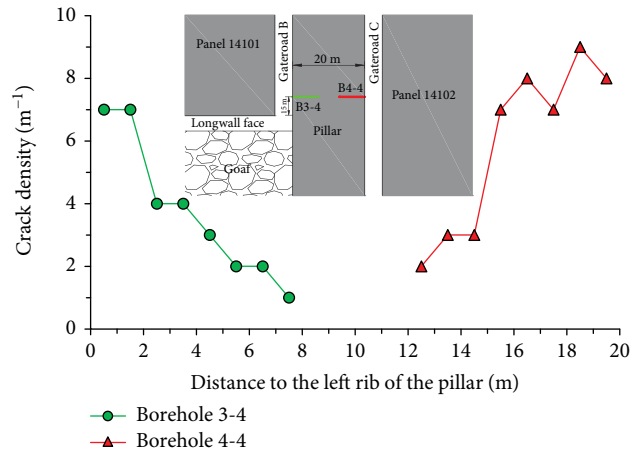

FIGURE 5: Fracture density observed by endoscope in a chain pillar (data from [2]).

number of field observations verify that a crushed zone exists near the boundary in some circumstances, such as soft coal pillar, deep mining, and high induced stress. Similarly, Salamon [64] reported that four distinct zones developed within a pillar, namely, elastic, yielding, crushed, and slumped zone.

The sizes of the distinct zones depend on the coal and rock strata properties, pillar dimension, support strategy, mining history, etc. In South Africa, Madden [65] conducted fracture monitoring of the sidewalls of pillars at Piet Retief and Longridge collieries in KwaZulu-Natal. His measurements showed that the depth of fracturing ranged from 1.5 m to 2.6 m in bord and pillar workings. As the excavation dimension increased, the fracture zones in the pillar could also substantially increase. Field observations [66] showed that the crushed zone, yield zone, and elastic zone in a 70 m wide pillar were 1 m, 4–5 m, and 58 m, respectively, after a 70 m wide panel was finished on one side of the pillar. However, for large-scale mining in adverse environments, a 40 m chain pillar could totally fail [67]. In connection to this, Bai et al. [2] conducted an advanced survey of fracture density in a chain pillar, as shown in Figure 5. They found that fractures were dense near the pillar ribs but gradually became sparse with increasing distance from the pillar boundary. Observations also showed that mining-induced stress played a significant role in fracture development. The fracture density increased as the face approached the measurement borehole and experienced a relatively larger increase in the area near the ribs compared with the core area.

Small-scale tests showed that the axial splitting failure mode occurred at low confining pressure, while the shear failure mechanism played a major role at high confining pressures [68]. Field observations in a Chinese coal mine also showed that splitting spalling failure usually occurred near the ribs where low confining pressure occurs [67], while shear failure usually occurred in deeper areas where high confining pressure was produced [2]. Mathey [69] conducted comparative tests on coal-concrete samples to study the relationship between failure (fracture mode) and the width-to-height ratios (aspect ratios). This research showed that samples with low aspect ratios (<2) failed in the typical

(a)

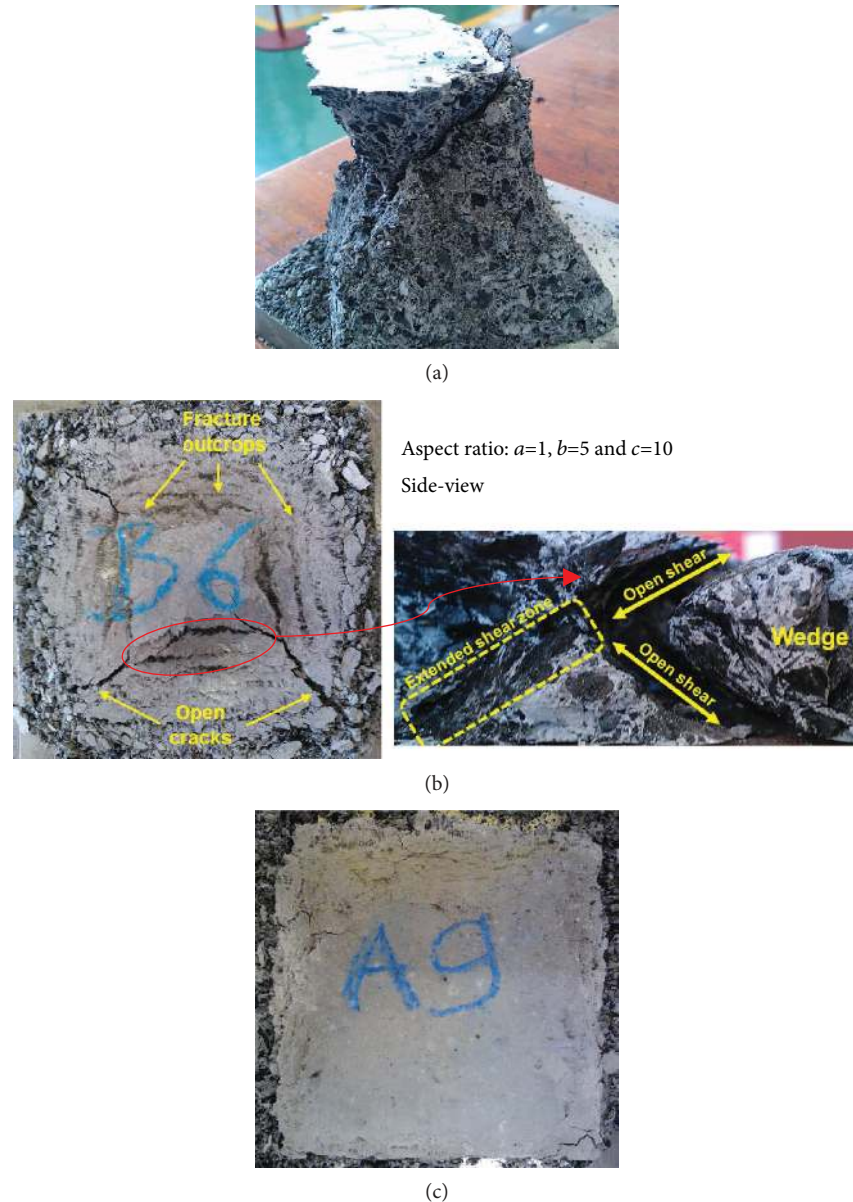Aspect ratio: $a=1$, $b=5$ and $c=10$

Side-view

(b)

(c)

FIGURE 6: Fracture modes for specimens with different aspect ratio (modified from [69]).

of double-cone fashion: the sidewalls of the sample fractured in a curved pattern to form the specimen into an hourglass shape, as shown in Figure 6(a). For specimens with aspect ratios of 3–6, brittle and brittle-ductile failures were observed. Open cracks approximately 1–2 mm wide near the sample boundaries were produced. Closer to the core, a series of near-linear fracture outcrops parallel to the four sidewalls were observed, as shown in Figure 6(b). Detailed analyses indicated that these fracture outcrops are shear fractures that yield a series of separated wedges with curved sides pointing toward the specimen center. Specimens with high aspect ratios (>6) showed ductile behavior. Localized fractures were concentrated near the sidewalls, as shown in Figure 6(c). Similar work on coal specimens [70] showed that the failure model also depends on interface friction.

Preexisting weak planes also have a significant effect on pillar behavior and failure. Owing to the complexity of the pillar system, numerical simulations are commonly used to demonstrate the interaction between newly generated and preexisting fractures in pillars [4, 71–73]. However, it was difficult to obtain a general conclusion on how the preexisting joints affected the pillar behavior and failure mode. This is because there are so many parameters that play a role in the system [4, 71–76], such as orientation and size of the joint sets, strength of the weak plane, distributions and density of the joints, failure mode of the inserted joints, confinement applied on the pillar, and pillar size.

In most laboratory tests and numerical simulations, single standing pillars were subjected to uniform vertical pressure. However, there are many observations and simulations illustrating that longwall mining-induced stress is not uniformly distributed in the pillar, and the stress varies with the mining process around the pillar [67, 77, 78]. As illustrated in [67], the hard immediate roofs caused nonuniform

TABLE 1: Parameters for predicting the height of the caved zone H_c.

Rock type	UCS (MPa)	Representative strata lithology	Parameters		
			a	b	σ
Hard and strong	>40	Quartz sandstone, limestone, sandy shale, conglomerate	2.1	16	2.5
Medium hard	20–40	Sandstone, argillaceous limestone, sandy shale, shale	4.7	19	2.2
Soft and weak	10–20	Mudstone, argillaceous sandstone	6.2	32	1.5
Weathered soft and weak	<10	Bauxite rock, weathered mudstone, clay, sandy clay	7.0	63	1.2

distributed vertical strain in the pillar, which was recognized as the primary factor causing the failure of the wide pillar (aspect ratio = 10.5).

4. Fractures in the Immediate Roofs or Top Coal

In most cases, the immediate roof strata are allowed to collapse behind the longwall face. The caved zone is generally highly fragmented with large porosity and high permeability. The height of the caved zone (H_c) is limited by the bulking factor (k) of the caved loose rocks and the mining height (h), which can be expressed as follows:

$$H_c = \frac{h}{k-1}. \qquad (1)$$

Peng and Chiang [15] reported that the sagging of the lowest uncaved strata (S_s) should also be taken into account.

$$H_c = \frac{h - S_s}{k-1}. \qquad (2)$$

This bulking factor-controlled caving model is widely used to calculate the caved zone height in engineering practice [18]. The rock bulking factor is larger if the rock strength is greater, which means that the coal seam with a weak roof has a larger ratio of the caved height and the mining height. Palchik [18] investigated the height of the caved zone in porous weak rock mass over shallow, abandoned underground coal mines (up to 80 m) by drilling in Donetsk, Ukraine. He reported that the caved height in weak porous rocks could reach 4.1–11.25 times the height of underground coal extraction. Recently, Palchik [19] has performed the comparison between the bulking factors and heights of the caved zones for very weathered (measurement of UCS is impossible, and, therefore, fracture intensity and quality of rocks were taken in consideration) and weathered (1 MPa < UCS < 11 MPa) rocks over shallow abandoned mines and for strong rocks (25 MPa < UCS < 150 MPa) at intermediate and large depths of longwall mining. Palchik [19] has shown that bulking of rocks is dependent not only rock strength but also on character (orderly or disorderly) of arrangement of rock fragments (debris) after rock collapse. It is found that very weathered rocks exhibit smaller values of bulking factor (1.06 < k < 1.165) and larger H_c/h =6.07-15.6 as compared with weathered rocks.

An empirical criterion predicting the extent of the caved zone has been developed in China with different lithological and geometric characteristics. For flat or nearly flat coal
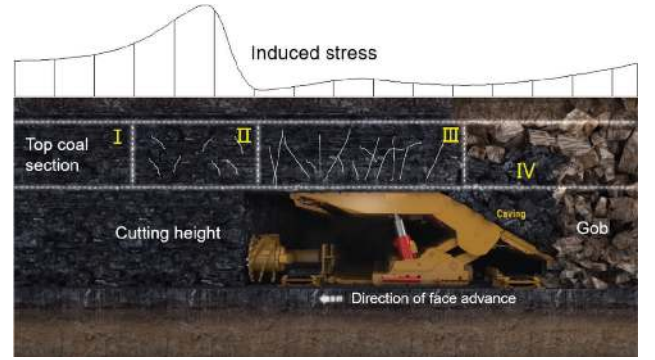

FIGURE 7: A conceptual model for longwall top coal status. I: the elastic zone, II: the deformed zone, III: the fractured zone, and IV: the broken zone.

seams, the height of the caved roof can be determined by the following equation [14]:

$$H_c = \frac{100h}{ah + b} \pm \sigma. \qquad (3)$$

In this equation, h is the accumulated mining height when using the sublevel mining method to extract a thick coal seam or the accumulated mining height of multiple seams. σ is the deviation that should be taken into account. a and b are coefficients depending on strata lithology, as listed in Table 1. It should be noted that the equation is adapted for single extraction with a thickness of 1–3 m or for multiple seam extraction with a total thickness less than 15 m.

Compared with fractures in the immediate roofs, researchers have paid much more attention to fractures in top coal because recovering top coal with high ratio is always difficult. It is widely believed that four different disturbed zones are produced in the top coal: the elastic zone, deformed zone, fractured zone, and broken zone, as shown in Figure 7. The elastic zone is outside the mining disturbed zone, where stress remains in its virgin state and the top coal is elastic. In the deformed zone, the top coal is compacted owing to the front abutment pressure. Cracks subperpendicular to the abutment stress could become closure, and horizontal dilatancy also occurs because of the relatively low horizontal restrict stress; therefore, cracks subparallel to the abutment stress may open and extend. In the fractured zone, the top coal is crushed into large fragments owing to the high differential stress and the repeated loading and unloading process by advancing shield supports. In the broken zone,
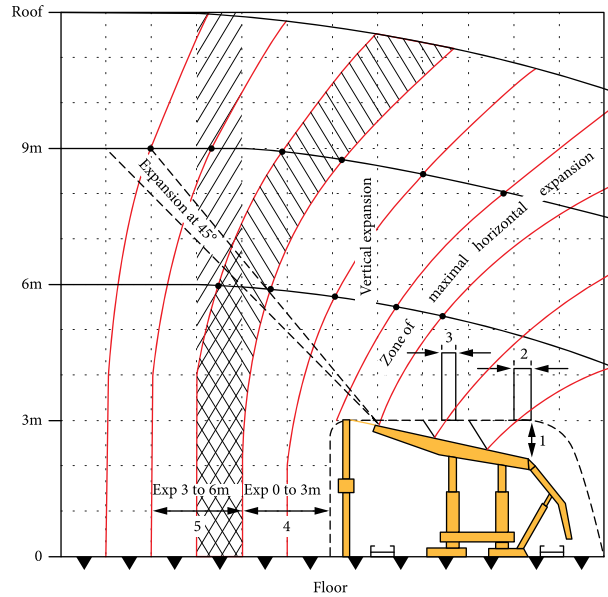
	Characteristics					Results of measurements					
Mines	Face	Seams	Depth (m)	Thickness (m)	Cutting height (m)	1	2	3	4	5	Expansion total %
Darcy	Taille D	4th	800	12.3	2.8	1155	254	120	0.38	3.35	20
Rozelay	T.3b	2nd	310	12	2.4	660	160	38		2.1	9
Ricard	Taille 2	1st	840	4.5	2.5	587	131		0	0.5	

Notes: Numbers in the Figure are the locations where the measurements were taken:

1. Convergence mm;
2. Convergence per metre of face advance;
3. Displacement of roof beams between setting and advancing;
4. Expansion 3 to 6m;
5. Expansion 0 to 3m

FIGURE 8: Field observations of top coal deformation and flow observed in French's coal mines in the 1960s and 1970s (after [154] and copying from [24]).

the crushed coal could further fragment during the caving process [7]. It should be noted that Figure 7 is a conceptual model for top coal status, but it varies depending on many factors such as coal seam characteristics, surrounding rock strata characteristics, stress conditions, longwall panel design, seam dip, preexisting weak planes, and groundwater [79–81].

Early research in France in the 1960s and 1970s produced a model of coal flow and corresponding displacements, as shown in Figure 8. It clearly shows that the top coal experiences small deformation in front of the longwall face, which rapidly increases behind the longwall face. Many investigations in Chinese mines have drawn similar conclusions. Measurements of top coal movement in a thick coal seam (average 16.8 m, maximum 20.0 m) showed that the initial displacement of the top coal occurred at a distance of eight times the cutting height (5 m) in front of the longwall face [82]. Horizontal deformation dominates the displacement in front of the longwall face. Vertical displacement plays a major role behind the longwall face. The same observations [81, 83, 84] of top coal deformation in Chinese coal mines yielded a similar profile. Fracture morphologies in the top coal varied with the altitude and locations in relation to the
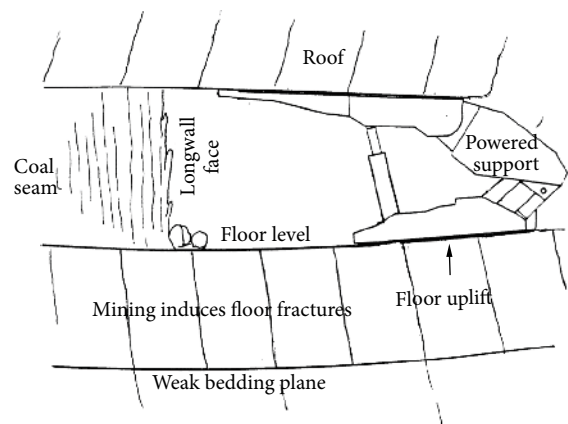

FIGURE 9: Primary failure-induced blocks in the floor and interaction with floor uplift to produce secondary failure [91].

active longwall face [85]. Vertical fractures at the front of the longwall face play a major role [85], while horizontal fractures are predominant behind the longwall face associated with the increase in aperture [86].
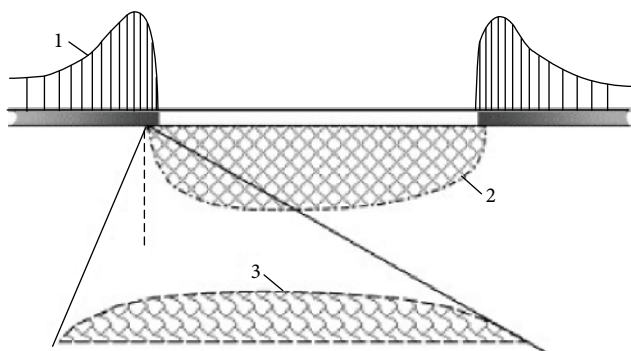
FIGURE 10: Fractured zone in the floor under longwall face (1: abutment pressure, 2: fractured zone, and 3: in situ hydraulic tensile fracture zone) [155].

5. Fractures in the Floors

Fractures in floor strata have not been studied to the same extent as roof fractures despite the fact that these cause significant delays in production [87]. The reason is because most of the time, floor failure is very difficult to measure owing to the nature of longwall operations [6]. Aghababaei et al. [88] identified three types of floor failure mechanisms. The first mechanism is puncturing of a weak floor if the stress below the shield supports exceeds the floor bearing capacity. The second mechanism is buckling of stratified rock floor due to the excessive lateral displacement of the coal seam toward the goaf. The third mechanism is compressive floor failure due to movement of multiple sliding blocks within the floor. Nemcik [87] defined the first and second mechanism as the primary failure and the third as the secondary floor failure. Stress concentrations ahead of the longwall face cause the primary floor failure, while secondary failure occurs as stress redistribution and displacement take place at or behind the face line after the floor is exposed. Field observations showed two main types of primary floor failure associated with two different floor fractures [89]: (a) shear failure along bedding planes in the floor, which causes horizontal fractures, and (b) formation of subvertical fractures parallel to the longwall face ahead of the longwall shield supports. Most of the time, primary failure occurs periodically as stress accumulates after a specific retreating of the coal face; however, continuous failure is also observed after each slice of coal is cut [89]. Observations of floor displacement and fractures in the floor [90] showed that vertical fractures play a dominant role within the failure zones. Numerical simulations using the continuum method [1] also showed a similar fracture profile in the floor.

As the longwall face retreats, stress relief occurs and unloaded floor strata may experience displacement. Secondary floor failure may consist of significant bending and bucking driven by localized stress concentration and displacements, which can lead to excessive floor heaving [87]. The primary fractures and bedding planes define the rock blocks within the floor, as shown in Figure 9. These blocks interact during the floor heave and dominate the secondary floor failure. The multiple sliding block model [91]

can be used to explain how the stress distribution develops within the broken floor.

In China, there are many mining practices for working above confined aquifers; hence, determining the failure scope in the floor is indispensable in such cases. Many observations show that the fracture zone in the floor [7] can be characterized as shown in Figure 10 along the face retreating direction. The failure zone rapidly develops into the floor behind the longwall face and then remains at the same level as it travels farther away from the goaf.

According to field tests, an empirical formula has been proposed [92] to predict the depth of the water-conducting failure zone.

$$H_f = 0.303 L_x^{0.8}, \tag{4}$$

where H_f is the depth of the water-conducting failure zone in the floor and L_x is the mining width of the mining face. It should be noted that the test data were collected from coal mines in Northern China with mining depths from 103 to 560 m.

In the longwall face width direction, the failure zone in the floor shows a different profile, as shown in Figure 11. The failure depth reaches the maximum level beneath the headgate and tailgate and slightly decreases in the central part of the longwall face. In addition, the profile heavily depends on the inclination of the coal seam. For inclined seams ($25° < \alpha < 60°$), the failure zone is asymmetric in the dip direction. The failure zone beneath the lower part reaches the maximum level and gradually decreases toward the upper part. The failure profiles shown in Figure 11 indicate that the maximum failure zone occurs beneath the roadways located on each side of the longwall face since high stress usually accumulates in these locations [67].

Although intensive research has been conducted on the scope of fractures in the floor, the results have not provided the characteristics of induced fractures, e.g., length distribution, orientations, aperture, and connectivity. These parameters are significant in order to evaluate the mechanical behavior of the floor rock and the seepage of water and gas.

6. Outstanding Issues

6.1. Field Observations. Field observation is the most effective method to determine the induced fractures, but it is also costly and time-consuming. The digital borehole camera recording method is widely used to observe fractures in the rock mass. Through continuous recording, this method can obtain 360° images of the borehole wall and determine the strike and dip of the fractures [26]. Image processing methods can be applied to the obtained images to identify fractures and quantify fracture patterns [93], making it possible to analyze huge image data within a limited time. Observation boreholes can be assigned at favorable locations to develop a model of the fracture network by extrapolating the observed fractures in single boreholes. Figure 12 shows an example of the observation of excavation-induced fractures around a circular tunnel in claystone conducted at the Meuse/Haute-Marne Underground Research Laboratory
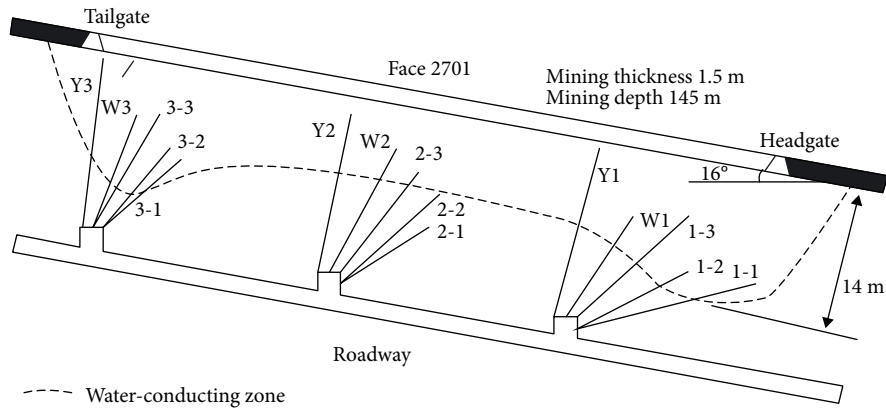
FIGURE 11: Observed profile of the water-conducting failure zone in the floor for slightly inclined coal seam ($0° < α < 25°$) in Fengfeng coal mines, Hebei Province [5].

(a)

Structures

☐ "Lower chevron fractures" $σ$H Major regional stress
☐ "Upper chevron fractures" $σ$h Minor regional stress
☐ "Tensile" fractures

(b)

FIGURE 12: Borehole observation of excavation-induced fractures (a) and the fracture network by extrapolating the observed fractures (b) around a circular tunnel at Meuse/Haute-Marne Underground Research Laboratory [94].
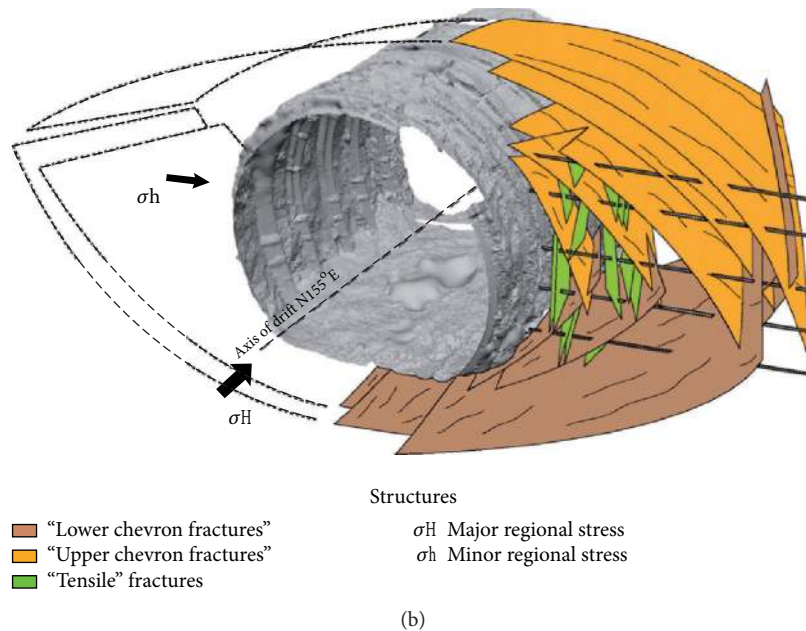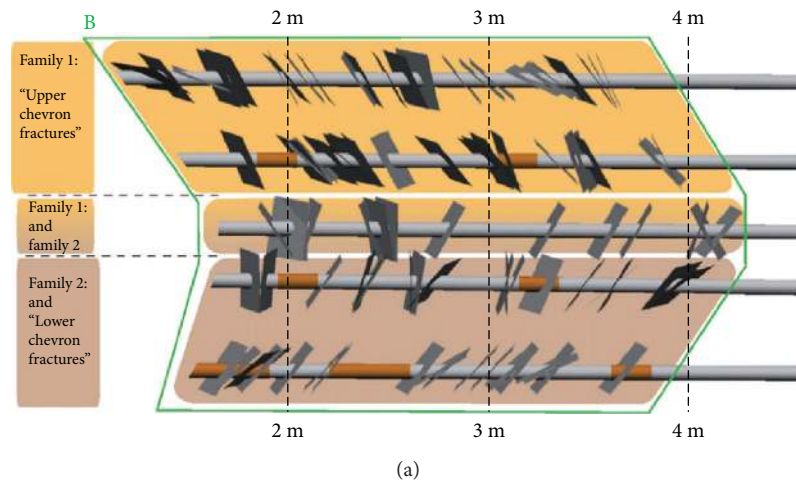
[94]. Similarly, several observations can be designed according to the retreating process of the longwall face to determine the evolution of the fracture network.

Although there are some observations of fracture distributions in the chain pillar [95–98], most are focused on the failure range of the pillar. Only a few works have studied the density distribution [2, 99], mainly because there is no demand for a detailed fracture profile of the pillar in most longwall activities. It is believed the fracture profile can be roughly determined using the method presented in [94]; however, additional difficulties could arise as the longwall face approaches the target site since the fractures develop rapidly and produce complex networks. Detailed fracture observations in the longwall face are not available because of the continuous operation of longwall mining. However, it is possible to extrapolate the fracture profile in the longwall face since most of the induced fractures are subparallel to the induced stress. In addition, fractures on the longwall face are relatively easy to measure because of the smooth face and good illumination. In a similar condition, fractures in the floor also have a simple profile because of the stress distribution; therefore, it is not very difficult to rebuild the fracture distributions if sufficient data is available. Until now, the borehole endoscope method [100, 101] is widely used to observe fracture distribution in the floor and it can provide fracture information not available from water-conducting observations [5]. However, it is expensive and time-consuming, especially for the fracture identification and morphology collection from so many images; this explains why few studies have been conducted in this field. In most cases, these works only focused on fracture depth and neglected fracture characteristics.

Compared with fracture distribution in the roof, floor, and chain pillar, fractures in the roof or top coal are more complex and variable. Using a borehole endoscope, Xie and Zhao [85] observed the fracture distributions in the top coal above the shield supports. They found that the fracture morphologies varied with the altitude in the top coal. Horizontal fractures were predominant in the bottom part of the top coal, and many vertical and inclined fractures also exist. In the upper part of the top coal, vertical fractures are ubiquitous, forming many strips. Fractures are sparse in the middle part of the top coal. According to field observation, Yan and Wu [86] stated that the number of fractures in the top coal exponentially increases as the longwall face approaches the measurement site. Space between the fractures also narrows during this process. The number of fractures oriented toward the vertical direction increased in front of the longwall face and decreased behind the longwall face. However, all of the observations could only provide a qualitative description of fracture distribution in the roof or top coal because the fracture network is too complex to obtain a quantitative description, let alone a similar fracture profile as shown in Figure 12. Compared with fractures in the rock mass, fractures on the roadway surface or longwall face are easier to observe. Xie et al. [102] measured the induced fractures on the roadway wall, which were used to evaluate the cavability of the top coal. In their study, they measured the fracture parameters (e.g., length, space, and orientation) manually.

However, the development of a remote detection technique [103] in recent years offers a promising alternative to manual measurements.

Recent advances in theory and available technology in image processing have greatly increased the ability to detect and characterize fractures in photo images [104]. Given the lower cost of digital cameras compared with laser scanners and their ease-of-use in the field, photogrammetry-based methods have been widely used for geotechnical characterization of rock slopes [28]. These have also been used to monitor underground deformation and pillar spalling in a limestone mine in the United States [105, 106]. Field practice has shown that this technique is capable of accurate measurements and fracture and joint detection. A practical test in an underground coal mine to perform rib characterization under poor lighting conditions showed that photogrammetry can be used in an underground environment and delivers results comparable to other measurement techniques [107]. Laser-based survey techniques (such as terrestrial LiDAR) are also widely used to capture fractures on rock (mass) surfaces [29, 108], but applications in underground coal mines have not yet been reported.

Stochastically generated fracture networks [109], which are commonly used to model natural fracture networks, could be a potential solution to rebuilding mining-induced fractures near the longwall panel. Stochastic discrete fracture networks (DFN) treat fracture properties (position, frequency, size, orientation, and aperture) as independent random variables that obey certain probability distributions determined from scan lines, window samples, and borehole imaging [110, 111]. The stochastic DFN method, which integrates the methods of the fractal geometry and power law models, can generate more realistic fracture systems; several studies have verified that the attributes of mining-induced fractures usually obey these distributions [102, 112, 113]. This improved DFN method can upscale fracture networks from small-scale fracture patterns [114, 115]. To ensure realistic fracture networks, field permeability and deformation data [77, 116] can also be used to calibrate the generated fractures.

6.2. Small-Scale Laboratory Tests. Small-scale laboratory tests are widely employed on coal measure samples to study mining-induced fractures and the associated mechanical and fluid behaviors. For example, cuboid coal samples under unconfined loading conditions are widely used to evaluate coal pillar strength and failure (or fracture) modes [69, 70]. In laboratory tests, measurement systems can be well prepared in order to obtain high-quality experimental data.

It is difficult to simulate the top coal fracturing process in the laboratory because current experimental techniques cannot realize the whole fracture process, from an intact sample to granular medium. However, several attempts have been made to do so. Song et al. [117] experimentally studied the relationship between coal fragment sizes and cover depth, coal strength, and discontinuities. The top coal cavability was evaluated according to the relationship in a specific site condition. Wang et al. [118] measured the velocity changes during UCS tests on top coal; therefore, a relationship can
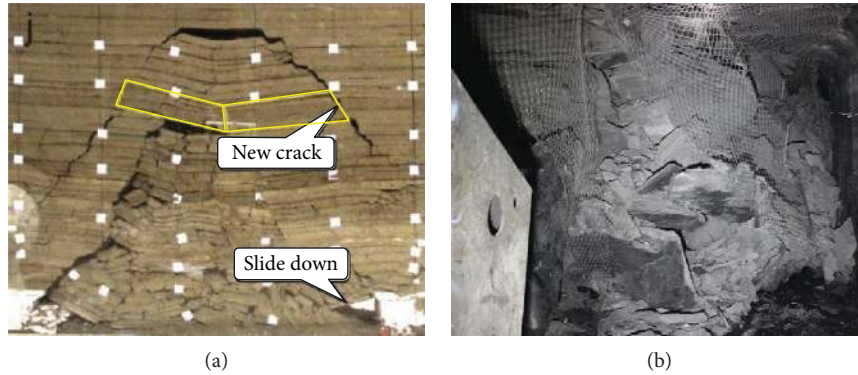
FIGURE 13: (a) Regular shape of caved fragments in a physical model of longwall mining [156]. (b) Field observations of the caved zone in a shallow buried coal seam with a thickness of 2.5 m.

be established between the velocity change and sample status (e.g., damage and mechanical behavior). This relationship can be used to evaluate the top coal status according to the measured velocity changes in the field.

Compared with the complex stress path in the roof, longwall face, floor, etc., the chain pillar experienced monotonic loading before it failed. Thus, UCS tests can be used to investigate coal pillar performance and the associated fracturing. Mathey [69] performed a series of tests on coal-concrete samples to study the relationships between failure (fracture mode) and aspect ratios, which have been summarized in Section 3. Many uniaxial tests were conducted on coal samples at West Virginia University with different aspect ratios and interface frictions to determine how these parameters affected the failure mode of the samples [70, 119]. It was found that interface friction has a significant effect on the failure mode, while the aspect ratio plays a secondary role. High interface strength with low aspect ratio may trigger bump failure of the pillar. However, in longwall mining, the induced stress across the chain pillar is not uniformly distributed; therefore, the degree to which the experimental results relate to field conditions is still unknown.

All of these conclusions came from the experimental monotonic loading conditions, whereas coal masses in the field experience quite a different stress path. Aside from the loading regime (e.g., UCS test), unloading also occurs, for example, the induced stress path in the top coal (Figure 7). It should be noted that unloading plays a primary role in top coal fracturing and fragmenting because the onset of unloading usually occurs behind the longwall face where fractures rapidly develop. Recently, Zhang et al. [120] numerically simulated the induced stress path in front of the longwall face. Then, the stress path was applied to cylindrical coal samples to observe the mechanical and permeability behaviors induced by longwall mining. They reported that the fracturing behavior and the associated permeability behavior from the stress path experiment differed from the results of typical conventional triaxial compression. Their results were comparable to the field tests results [116, 121]. Using CT scanning and 3D reconstruction techniques, the microstructure and fracture connectivity can be characterized [122] and quantitatively described by the fractal theory [123]. By placing the test chamber inside a CT facility,

fracture development can be continuously monitored at different stages of loading during the tests [112].

However, there are also some limitations. Most of the laboratory tests were conducted under the monotonic loading regime, but longwall retreating also produces unloading processes, e.g., in most circumstances, the rock mass surrounding the longwall face experiences a specific stress path. Stress path-based tests on coal mechanical and permeability behaviors have shown different results from conventional triaxial tests [120]. Another limitation is that the small-scale sample does not contain sufficient geological information. Therefore, the test results provide data on intact rock properties and not on rock mass properties. Although rock properties can be converted into rock mass properties according to rock mass classification systems [124], this method cannot fully reflect the effect of preexisting weak planes on rock mass fracturing. In addition, in most engineering practice, the direction of the stress also varies, which cannot be recreated in existing laboratory experiments. Defects or the induced fractures in top coal can take advantage of stress rotations to extend in their favored directions [125]. Therefore, laboratory results could underestimate the fracture network in the sample because tests often use small samples that do not provide enough information about preexisting weak planes.

6.3. Laboratory Physical Modeling. Physical modeling has proven to be a useful tool for intuitively illustrating mining-induced fracture propagation, caving process, ground movements, and roof structures. Many successful cases have been reported for characterizing induced fractures by thick coal seam extraction or LTCC mining [17, 21, 126], inclined coal seam extraction [22, 127], and multiseam mining [128, 129]. In most cases, small-scale physical models (usually less than $1:100$) were developed because of the large dimensions of the longwall mining profile. The small-scale models are capable of simulating fracturing and ground movements of roof strata from a global-scale view, but it is very difficult to illustrate the complex fracture process in the areas of interest. For example, most physical models cannot reproduce the irregular falling of caved zones, as shown in Figure 13(a). Field observations in Figure 13(b) clearly show that goaf materials in the caved zone are highly fragmented and broken into
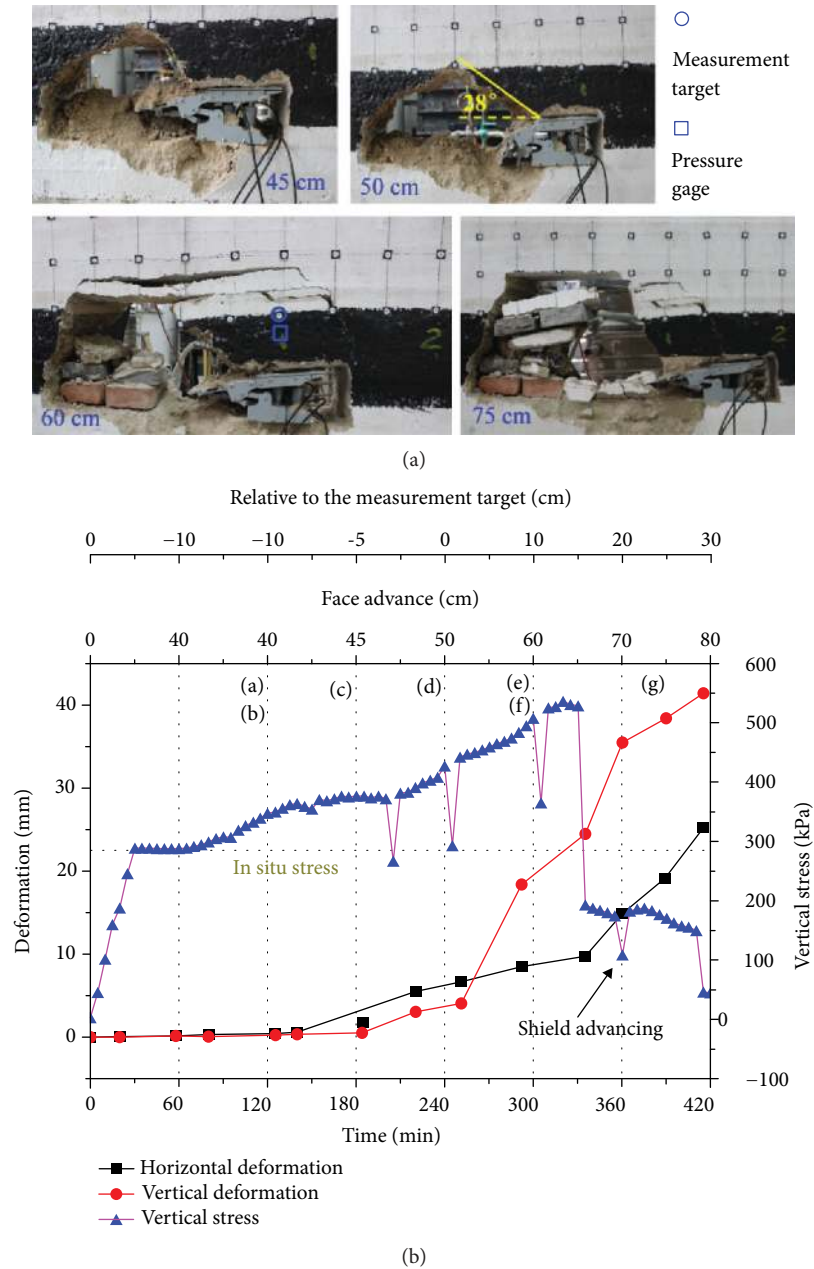
(a)

(b)

Figure 14: (a) Physical modeling of the whole process of top coal caving and (b) top coal deformation and vertical stress in relation to time and longwall face advancements. The corresponding top coal status in (a) is also marked.

irregular shapes of various sizes. Under certain unfavorable conditions, the immediate roofs cannot rupture into fragments, but horizontally separate and fall onto the floor with sparse vertical fractures [130]. Regular-shaped fragments and poorly fragmented pieces result in a smaller bulking factor of the caved material, indicating that the physical model could produce a larger caved zone and overestimate the height of the fractured zone. Infillings like foam material can be used to fill in the caved zone to offset the underestimated bulking factor after careful calculation [126].

Using large-scale models, mining-induced fracture can be well illustrated. We have shown that the large-scale

physical models (1 : 50) can simulate the fracturing and caving process [126] using a developed construction material. This construction material consists of a mixture of sand, gypsum, and crushed stones and can truly display the whole caving process of the top coal. A physical model was constructed according to the geological and mining conditions of an LTCC face. The caving process and the associated stress and deformation of the top coal are shown in Figure 14. It is clear that the top coal deformed in front of the longwall face. The deformation increased as the face advanced and passed with increasing vertical stress, which is favorable for top coal fragmentation. The top coal caved immediately after

the shield. It can be seen that the physical model successfully reproduced the caving process, from intact to granular medium associated with the fracturing of the roofs. The induced stress and deformation of the top coal also agreed well with field observations. Using very large-scale physical models (1 : 17.5), Guo [131] studied the effects of preexisting joints on the stability of the very high longwall face. In the physical modeling, the effects of the joint inclination and azimuth angle and joint space on the development of fractures in the longwall face were carefully observed for both hard and soft coal seams. The observations showed that the large-scale physical models were able to reproduce the development of fractures in the longwall face, and several typical fracture profiles that usually occur in the field were summarized.

In most cases, physical modeling does not take the horizontal stress into account. On the one hand, it is not easy to apply horizontal stress to a huge model; on the other hand, horizontal stress may cause instability since the model is thin (usually 20–30 cm). One physical model and numerical simulation have shown that horizontal stress concentration may be a major cause of roof collapse [17]. The other horizontal stress perpendicular to the plane is also not available. Therefore, the 2D physical model can only simulate field conditions that can be simplified into 2D problems, which means that fracture profiles in the 3D space cannot be accurately reproduced. To overcome these limitations, the 3D physical models were developed to simulate longwall mining-induced rock mass responses [132–135]. However, it is very difficult to obtain the fractures inside the model. Therefore, rock mass deformation and stress changes are still the monitoring parameters used to characterize the rock mass performance [132, 133]. By removing a portion of the 3D model after the simulation, the induced fractures in the roof can be observed [134, 135]. However, this brings up another question: how can we distinguish the induced fractures and secondary fractures produced during the removal process. Although there are no effective ways to extract fractures inside the model, 3D physical modeling provides an advanced method to simulate longwall mining-induced fractures under more realistic in situ conditions.

The raw materials constituting the construction material also affect the fracture characteristics of the physical model. Although this subject does not attract enough attention, experimental studies in [136] have shown the effect of sand grain size on mining-induced fractures in the physical model and found that fracture density was higher when using coarser sand to produce the construction material.

6.4. Numerical Modeling. Numerical simulations are popular for characterizing mining-induced fractures. Although the continuum models are widely used, they are not suitable for representing fractures because the element size should be very fine to illustrate fracture development by zone failure [38, 44], especially for large excavations such as longwall retreating simulation. In addition, the continuum models require a well-developed algorithm to implicitly represent the caving progress, goaf consolidation, and retreating

process [137, 138]. When fine zones are employed, the continuum models can simulate mining-induced fractures, which are usually illustrated by strain/failure band, stress and failure zone distribution, or shear displacement. Using the FLAC 2D models, we successfully reproduced the tensile splitting and shear slipping failure [38, 44] of the longwall face. In the simulations, tensile splitting failure was represented by the tensile stress and deformation distribution, while the shear slipping failure was illustrated by the shear bands. Nemcik [87] also used the FLAC 2D model to study the floor failure. In the modeling, shear displacement contours were employed to recognize the shear fractures below the shield support. The subvertical fractures were found to dip at steep angles of 70°–90° toward the goaf, which agreed well with in situ observations. The mechanical mechanism (e.g., stress distribution) was clarified using the competent model, which was not available from field observations. Using a 3D continuum model, Yasitli and Unver [139] studied the movement and failure zone in the top coal using high-level LTCC (i.e., recovery window embedded in the canopy) and concluded that the top coal within 1.5 m above the shield supports was well fractured. Above the fractured part, the top coal was either not fractured or fractured into large blocks. However, owing to the sparse elements, fracture development in the top coal cannot be presented.

The discontinuum models may be a good choice to represent the physics of the problem. The DEM models with finer blocks in the region of interest have shown good representation of longwall top coal caving [81, 140] and fracture development in roofs [141, 142]. By introducing Voronoi or triangular blocks in a small region of interest, fracture development induced by large-scale longwall retreating can be represented more realistically. These applications include fracture characteristics in the longwall face [53], damage development in top coal [126], and brittle fracture and damage development along an unstable goaf [143]. Vakili and Hebblewhite [81] investigated the factors affecting top coal cavability. However, their work did not show the fracturing process of top coal. Le et al. [140] investigated the top coal caving mechanism by a DEM model. In the model, the blocks were assigned strain-softening properties to obtain the intact rock failure. The simulations indicated that bedding planes mainly showed shear failure, while vertical joints experienced tensile failure. The top coal predominantly experienced shear failure, which is in accordance with the results in [139] using the continuum models. By introducing Voronoi polygonal blocks to represent the rock mass, we modeled the damage evolution in the top coal [126], which was defined as the ratio of the failed contact number and the total contact number in each subsection within a certain range in the top coal. To illustrate the damage development, the damage and induced stress in the top coal were calculated. It is clearly shown that the induced stress in the top coal gradually increased as the longwall face approached the monitoring sites and quickly decreased as the longwall face passed the sites. The peak stress is located immediately in front of the longwall face. The stress distribution is consistent with the results of the continuum models [144]. As the damage in each site steadily increased, a more rapid increase was observed after the peak

(a) (b)

Intact rock bonded particle model

SRM

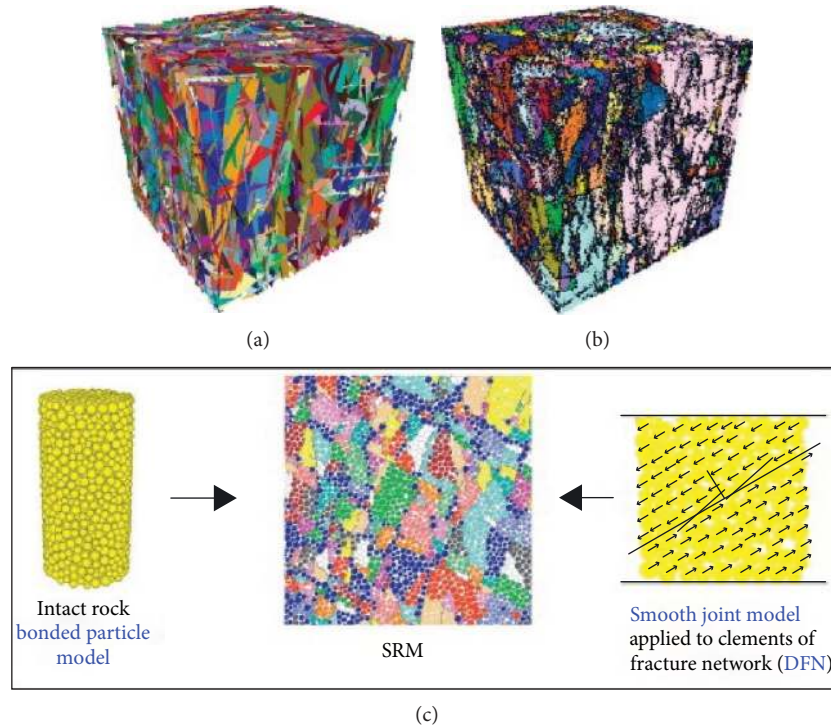Smooth joint model applied to elements of fracture network (DFN)

(c)

Figure 15: The synthetic rock mass (SRM) model [149]. (a) The discrete fracture network (DFN) model, (b) the corresponding synthetic rock mass sample, and (c) synthetic rock mass basic components.

stress location. The lowest part of the top coal has larger damage (i.e., larger fracture density) compared with the upper parts, which agrees with field observation that the lower parts of the top coal usually fragment into smaller pieces. However, few block separations were observed. For tensile fractures between blocks, most separations are less than 0.001 m, causing poor display performance of fractures in such a large model. This may result from the discordance intrinsic to the DEM model used. High damping was employed in the simulation to ensure calculation stability, i.e., the model calculates in a static state. However, field practice shows that top coal fragmenting and caving are dynamic mechanisms that occur in the section behind the shield supports since the top coal is free to fail and cave. We did not integrate the preexisting weak planes in our model, which are ubiquitous in coal seams. Although the natural fractures in coal seams have been fully studied [145, 146], their effects on fracture development have not been well considered under longwall mining conditions.

The hybrid continuum/discontinuum models, which share similar ability as DEM to represent fracture development, have been successfully employed to simulate the mass block caving process and surface subsidence [37, 147]. Therefore, the hybrid method can also be applied to investigate longwall mining-induced fracture behaviors. Recently, a GPU-accelerated technique was developed to reduce computational costs, making it more efficient to run larger and higher resolution simulations [148].

It is easy to take discontinuities into account in the DEM or hybrid models. Field discontinuities could come from field survey results, but the DFN models are frequently used. A

DFN is a computational model that explicitly represents the geometric properties of fracture networks. The DFN models can be generated from geological mapping, stochastic realization, or geomechanical simulation to represent different types of rock fractures [109]. When detailed discontinuities are considered, the model requires a high resolution. Under such circumstances, field-scale models are too large to run. Therefore, a small-scale synthetic rock mass (SRM) model of the site of interest can be a viable alternative [149]. This model uses the bonded particle model for rocks to represent intact material and the smooth-joint contact model to represent the in situ discontinuity network, as shown in Figure 15. Thus, the rock mass response is determined from the combined behavior of intact material and discontinuities (which include the interaction between the intact rock and joints). The stress path in a specific site, which can be obtained from field measurement or simple simulations, can be applied to the SRM model to reproduce the desired engineering activity. The spherical SRM model can be used to apply complex stress paths that involve changes in both magnitude and orientation [149]. The application of such a model showed realistic rock mass disintegration processes and had good agreement with observations of fragmentation sizes for a block caving simulation [149]. Therefore, if the computational cost is acceptable, the field-scale models are the preferred option. Medhurst et al. [150] simulated the LTCC process using a hybrid FLAC/PFC model. In the hybrid model, the FLAC model was used to simulate the far-field stress, and the embedded PFC model was used to simulate the caving process of the top coal and immediate roofs. Joints and cleats were considered in the model based on the SRM

approach. The hybrid models containing DFN were also successfully used to simulate block caving [37, 147].

6.5. Comparative Analysis. Compared with other methodologies, field observation is undoubtedly the most effective method to capture the longwall mining-induced fractures. Borehole observation is a mature method that is widely used to obtain fracture information in the rock mass. It provides useful information on fractures (e.g., fracture spaces, orientations, and apertures) but has difficulty estimating the fracture sizes and connectivity. The digital borehole camera and image processing method make it easier to capture the fractures in huge image data and determine the strike and dip. However, it is cost-intensive and time-consuming; sometimes it is difficult to gain access to certain locations, e.g., the longwall face and floor in the goaf. In addition, digital borehole camera and borehole digital optical televiewer do not always have high technical specifications (CCD pixels, spatial precision, color (in bits), etc.) and, therefore, fractures may be overlooked in case when filling material (debris of rock matrix) in fracture space and rock mass are of the same color [151]. Owing to its low cost and easy accessibility, photogrammetry-based methods are a potential technique to capture fractures on rock mass surfaces, e.g., longwall face and tunnel boundaries. It can also provide information on fracture sizes and connectivity, which are usually not available in borehole observations. Therefore, it is the preferred method when the focus is on fracture close to boundaries under good lighting conditions. Geographic information system (GIS), DNF, and similar methods could provide a means to extrapolate and digitize fracture networks based on the aforementioned data [109, 152, 153].

For small-scale laboratory experiments, intensive monitoring systems could be employed to record the rock sample responses (stress, strain, permeability, velocity changes, etc.) under controlled conditions. Some of the measurements are difficult or cannot be performed in the field. Using CT scanning and 3D reconstruction techniques, the produced fractures can be well characterized during/after the tests. However, it is difficult to relate experimental results to field conditions, even if similar stress paths are employed in the experiments. This is because the stress rotation and tensile stress in the tests are still not available, which have shown a significant effect on rock fracturing. Moreover, small samples cannot contain enough natural weak planes to represent the rock mass. If the number of preexisting weak planes are few, laboratory tests are a good choice for those interested in the qualitative characteristics of mining-induced fractures.

Compared to small-scale tests, physical modeling can provide more field information such as bedding planes, joints, shield support, and even aquifers. Many cases have proven its capacity to model roof movement and fracture development. Large-scale geometric models are recommended if detailed fracture characteristics are needed, such as fracture development in the top coal, pillar, and longwall face. Simple geological structures (e.g., bedding planes, faults, and main joints) can also be introduced into the physical model. Photogrammetry makes it easy to capture the induced

fracture networks and movement fields. If horizontal stress can be applied to the physical model, then it can mimic field conditions in a more realistic manner. Compared with the 2D models, the 3D physical models show greater correspondence with field conditions. However, until now, there are no effective methods to obtain the fractures inside the model. For physical modeling, the most important issue is to find applicable construction materials to better illustrate the development of fractures.

Continuum numerical methods are a poor choice when modeling mining-induced fractures owing to their inability to simulate complex fracture system. The discontinuum and hybrid continuum/discontinuum models are a better choice to simulate longwall retreating and induced fractures. Element sizes are critical for simulating fractures. However, it is time-consuming or even impossible to build a large-scale model with very fine elements. Thus, emphasis can be placed on a relatively small region of interest. With the rapid development of computing powers and accelerated techniques, large geomechanical models are increasingly adopted. Structural elements can also be introduced in numerical models and are well represented if sufficient data are collected from the field and proper constitutive models are employed. Therefore, the discontinuum models are always not a poor choice for simulating mining-induced fractures. However, finding an effective method that can determine the appropriate properties to represent realistic objectives (e.g., rock mass and geology structures) is an issue that still needs to be resolved.

7. Concluding Remarks

After a general introduction of longwall mining-induced fractures from a global perspective, the present review summarized the studies on induced fractures in near-face regions, e.g., fractures in the longwall face, chain pillar, immediate roof and top coal, and floor. For brittle and hard coal seams, there are two major fracture profiles: (a) fine fractures parallel to the longwall face, which usually produce tensile splitting failure with laminae, and (b) separated shear fractures that obliquely develop into the longwall face, which can produce shear slipping failure with large blocks. For soft coal seams, crushed squeezing failure was usually observed, indicating that induced fractures are ubiquitous. It is believed that tensile fractures parallel to the coal pillar boundaries frequently occur, while shear fractures develop between the core and tensile failure zones. Therefore, slender pillars usually fail in an hourglass shape, while gradual shear failure is usually observed for squat pillars. Preexisting weak planes, surrounding rock strata, and coal seam properties and the interface between them have significant effects on fracture distributions in chain pillars. Therefore, fracture profiles in chain pillars are strongly case-dependent, making it difficult to arrive at a general conclusion; more field observations and laboratory tests are needed. Fractures in the immediate roof and top coal are ubiquitous and strongly affected by the mining-induced pressure in the roof. In almost all cases, the roof or top coal fragmented into small pieces behind the longwall face with a height of 4 to 20 times the thickness

of the extracted coal seam. Therefore, it is impossible to obtain all the fracture profiles if the site of interest is near the longwall face. In general, vertical fractures play a major role in front of the face, while horizontal fractures are predominant behind the longwall face, where vertical displacement rapidly increases. From the limited field observations and laboratory experiments, fractures in the floor were less developed as those in the coal seam and immediate roofs. Failures rapidly increased near the longwall face and then remained at the same level with increasing distance into the goaf. In the longwall face width direction, fracture zones in the floor reached the maximum level beneath the panel boundaries and slightly decrease in the central part of the panel, but the fracture profiles depended on the incline of the coal seam. In general, there are two different floor fractures: (a) shear failure along bedding planes and (b) subvertical fractures that form parallel to the longwall face. This summary was based on limited field observations because floor fractures have not been studied to the same extent as roof fractures owing to the difficult measurement of operations. More filed observations are needed to verify the current conclusions and obtain general results.

Different approaches, including field observation and detection, laboratory tests, physical modeling, and numerical simulations, which are generally employed to investigate induced fractures, were surveyed. Some of the outstanding issues that need to be addressed when using these approaches were discussed. Field observation is the most effective method to capture the longwall mining-induced fractures. Borehole observation, although improved by the use of continuous digital cameras and image processing, still provides limited useful information, e.g., 3D geometries of the induced fractures. By using GIS, DNF, and similar methods, it is possible to extrapolate and digitize fracture networks if sufficient data are collected. Small-scale laboratory experiments, which could provide accurate fracture temporal-spatial distributions by intensive monitoring and detection equipment, remain a poor choice to investigate longwall mining-induced fractures. It is difficult to relate experimental results to field conditions owing to the inconsistent stress state used in the laboratory. Moreover, it is also impossible to consider natural structural elements in a small sample, which has shown significant effects on induced fractures. Physical modeling can introduce more field information; therefore, it could better represent field conditions. The large-scale physical models are recommended if detailed fracture characteristics are needed in a limited scope. The capacity of the physical model could be improved if horizontal stress can be introduced in the 2D models. For the 3D models, mature techniques are required to easily capture the induced fractures inside the model. Construction materials, which determine the capacity of the physical model to simulate fracture development, require more attention. The discontinuum numerical models are a promising method to simulate longwall mining fractures. However, ways to simplify complex realistic conditions and determine the parameters and constitutive models for geomechanical elements have not been fully addressed. With the rapid development of this technology, it is expected to attract increased attention.

Characterizing mining-induced fractures in near-face regions is always a challenging task because fracture sizes in these regions range from several meters to micrometers; hence, it is difficult to find a common technique or method to observe and characterize these fractures in such a large scope. Most of the time, we identify the fracture size of interest and the associated investigation methods according to the problem we intend to study. As the primary mechanism in controlling the stability of rock masses and finding feasible solutions, on all scales, the induced fracture characteristics of surrounding rocks will remain a topic of interest in underground longwall mining, and methods to capture and characterize the fracture profiles will continue to be developed.

Conflicts of Interest

The authors declare that they have no conflicts of interest.

Acknowledgments

References

[1] Y. Heritage, W. Gale, and A. Rippon, "Connectivity of mining induced fractures below longwall panels: a modelling approach," in *Proceedings of the 17th Coal Operators' Conference, University of Wollongong*, pp. 41–50, Australia, 2017.

[2] Q.-S. Bai, S.-H. Tu, F.-T. Wang, X.-G. Zhang, H.-S. Tu, and Y. Yuan, "Observation and numerical analysis of the scope of fractured zones around gateroads under longwall influence," *Rock Mechanics and Rock Engineering*, vol. 47, no. 5, pp. 1939–1950, 2014.

[3] Q.-S. Bai, S.-H. Tu, C. Zhang, and D. Zhu, "Discrete element modeling of progressive failure in a wide coal roadway from water-rich roofs," *International Journal of Coal Geology*, vol. 167, pp. 215–229, 2016.

[4] D. Elmo and D. Stead, "An integrated numerical modelling–discrete fracture network approach applied to the characterisation of rock mass strength of naturally fractured pillars," *Rock Mechanics and Rock Engineering*, vol. 43, no. 1, pp. 3–19, 2010.

[5] J. Zhang, "Investigations of water inrushes from aquifers under coal seams," *International Journal of Rock Mechanics and Mining Sciences*, vol. 42, no. 3, pp. 350–360, 2005.

[6] S. S. Peng, *Longwall Mining*, Society for Mining, Metallurgy, and Exploration, Inc. (SME), Englewood, CO, USA, 2nd edition, 2006.

[7] M. Qian, P. Shi, and J. Xu, *Underground Pressure and Strata Control*, China University of Mining and Technology Pressure, Xuzhou, China, 2010.

[8] P. Tammetta, "Estimation of the change in storage capacity above mined longwall panels," *Groundwater*, vol. 54, no. 5, pp. 646–655, 2016.

[9] C. Ö. Karacan, "Prediction of porosity and permeability of caved zone in longwall gobs," *Transport in Porous Media*, vol. 82, no. 2, pp. 413–439, 2010.

[10] V. Palchik, "Formation of fractured zones in overburden due to longwall mining," *Environmental Geology*, vol. 44, no. 1, pp. 28–38, 2003.

[11] H. Wang, D. Zhang, X. Wang, and W. Zhang, "Visual exploration of the spatiotemporal evolution law of overburden failure and mining-induced fractures: a case study of the Wangjialing coal mine in China," *Minerals*, vol. 7, no. 3, p. 35, 2017.

[12] F. Wang, S. Tu, C. Zhang, Y. Zhang, and Q. Bai, "Evolution mechanism of water-flowing zones and control technology for longwall mining in shallow coal seams beneath gully topography," *Environmental Earth Sciences*, vol. 75, no. 19, p. 1309, 2016.

[13] D. Xuan and J. Xu, "Longwall surface subsidence control by technology of isolated overburden grout injection," *International Journal of Mining Science and Technology*, vol. 27, no. 5, pp. 813–818, 2017.

[14] State Bureau of Coal Industry, *Regulations for Setting Coal Pillar and Mining Pressed Coal Under Buildings, Water Bodies, Railways, and Main Roadway*, China Coal Industry Publishing House, Beijing, China, 2000.

[15] S. Peng and H. Chiang, *Longwall Mining*, Wiley, New York, NY, USA, 1984.

[16] M. Bai, F. S. Kendorski, and D. J. Van Roosendaal, "Chinese and North American high-extraction underground coal mining strata behavior and water protection experience and guidelines," in *Proceedings of the 14th International Conference on Ground Control in Mining*, pp. 209–217, Morgantown, WV, USA, 1995.

[17] H. Kang, J. Lou, F. Gao, J. Yang, and J. Li, "A physical and numerical investigation of sudden massive roof collapse during longwall coal retreat mining," *International Journal of Coal Geology*, vol. 188, pp. 25–36, 2018.

[18] V. Palchik, "Influence of physical characteristics of weak rock mass on height of caved zone over abandoned subsurface coal mines," *Environmental Geology*, vol. 42, no. 1, pp. 92–101, 2002.

[19] V. Palchik, "Bulking factors and extents of caved zones in weathered overburden of shallow abandoned underground workings," *International Journal of Rock Mechanics and Mining Sciences*, vol. 79, pp. 227–240, 2015.

[20] J. Ju and J. Xu, "Structural characteristics of key strata and strata behaviour of a fully mechanized longwall face with 7.0 m height chocks," *International Journal of Rock Mechanics and Mining Sciences*, vol. 58, pp. 46–54, 2013.

[21] J. Ju and J. Xu, "Surface stepped subsidence related to top-coal caving longwall mining of extremely thick coal seam under shallow cover," *International Journal of Rock Mechanics and Mining Sciences*, vol. 78, pp. 27–35, 2015.

[22] X. Li, Z. Wang, and J. Zhang, "Stability of roof structure and its control in steeply inclined coal seams," *International Journal of Mining Science and Technology*, vol. 27, no. 2, pp. 359–364, 2017.

[23] G. Fan, D. Zhang, and X. Wang, "Mechanism of roof shock in longwall coal mining under surface gully," *Shock and Vibration*, vol. 2015, Article ID 803071, 8 pages, 2015.

[24] J. M. Galvin, *Ground Engineering - Principles and Practices for Underground Coal Mining*, Springer, Cham, Switzerland, 2016.

[25] S. S. Peng, *Coal Mine Ground Control*, Society for Mining, Metallurgy, and Exploration, Inc. (SME), Englewood, CO, USA, 3rd edition, 2008.

[26] S. J. Li, X. T. Feng, C. Y. Wang, and J. A. Hudson, "ISRM suggested method for rock fractures observations using a borehole digital optical televiewer," *Rock Mechanics and Rock Engineering*, vol. 46, no. 3, pp. 635–644, 2013.

[27] C. Wang and K. T. Law, "Review of borehole camera technology," *Chinese Journal of Rock Mechanics and Engineering*, vol. 24, no. 19, pp. 3440–3448, 2005.

[28] D. Tannant, "Review of photogrammetry-based techniques for characterization and hazard assessment of rock faces," *International Journal of Geohazards and Environment*, vol. 1, no. 2, pp. 76–87, 2015.

[29] M. J. Lato and M. Vöge, "Automated mapping of rock discontinuities in 3D lidar and photogrammetry models," *International Journal of Rock Mechanics and Mining Sciences*, vol. 54, pp. 150–158, 2012.

[30] B. N. Whittaker, P. Gaskell, and D. J. Reddish, "Subsurface ground strain and fracture development associated with longwall mining," *Mining Science and Technology*, vol. 10, no. 1, pp. 71–80, 1990.

[31] T. N. Singh and I. W. Farmer, "A physical model of an underground coal mine prototype," *International Journal of Mining Engineering*, vol. 3, no. 4, pp. 319–326, 1985.

[32] B. Ghabraie, G. Ren, X. Zhang, and J. Smith, "Physical modelling of subsidence from sequential extraction of partially overlapping longwall panels and study of substrata movement characteristics," *International Journal of Coal Geology*, vol. 140, pp. 71–83, 2015.

[33] L. Jing, "A review of techniques, advances and outstanding issues in numerical modelling for rock mechanics and rock engineering," *International Journal of Rock Mechanics and Mining Sciences*, vol. 40, no. 3, pp. 283–353, 2003.

[34] L. Jing and J. A. Hudson, "Numerical methods in rock mechanics," *International Journal of Rock Mechanics and Mining Sciences*, vol. 39, no. 4, pp. 409–427, 2002.

[35] L. Jing and O. Stephansson, *Fundamentals of Discrete Element Methods for Rock Engineering: Theory and Applications*, Elsevier, Amsterdam, Netherlands, 2007.

[36] A. Lisjak and G. Grasselli, "A review of discrete modeling techniques for fracturing processes in discontinuous rock masses," *Journal of Rock Mechanics and Geotechnical Engineering*, vol. 6, no. 4, pp. 301–314, 2014.

[37] D. Elmo, D. Stead, E. Eberhardt, and A. Vyazmensky, "Applications of finite/discrete element modeling to rock engineering problems," *International Journal of Geomechanics*, vol. 13, no. 5, pp. 565–580, 2013.

[38] Q.-S. Bai, S.-H. Tu, X.-G. Zhang, C. Zhang, and Y. Yuan, "Numerical modeling on brittle failure of coal wall in longwall face—a case study," *Arabian Journal of Geosciences*, vol. 7, no. 12, pp. 5067–5080, 2014.

[39] Y. Yong, T. Shihao, W. Qi, M. Xiaotao, T. Hongsheng, and S. Lulu, "Mechanics of rib spalling of high coal walls under fully-mechanized mining," *Mining Science and Technology*, vol. 21, no. 1, pp. 129–133, 2011.

[40] Y. Pang and G. Wang, "Hydraulic support protecting board analysis based on rib spalling "tensile cracking-sliding" mechanical model," *Journal of China Coal Society*, vol. 42, no. 8, pp. 1941–1950, 2017.

[41] G. Song, S. Yang, and Z. Wang, "Longwall face stability analysis using Ritz method and its 3D physical modelling study," *Journal of China Coal Society*, vol. 43, no. 8, pp. 2162–2172, 2018.

[42] B. Fu, M. Tu, and M. Gao, "Study on unloading instability model of working face with large mining height," *Journal of Mining & Safety Engineering*, vol. 34, no. 6, pp. 1128–1133, 2017.

[43] S. Luo, Y. Wu, K. Liu, X. Panshi, and W. Hongwei, "Asymmetric load and instability characteristics of coal wall at large mining height fully-mechanized face in steeply dipping seam," *Journal of China Coal Society*, vol. 43, no. 7, pp. 1829–1836, 2018.

[44] Q.-S. Bai, S.-H. Tu, M. Chen, and C. Zhang, "Numerical modeling of coal wall spall in a longwall face," *International Journal of Rock Mechanics and Mining Sciences*, vol. 88, pp. 242–253, 2016.

[45] R. C. Frith, "A holistic examination of the load rating design of longwall shields after more than half a century of mechanised longwall mining," *International Journal of Mining Science and Technology*, vol. 25, no. 5, pp. 687–706, 2015.

[46] J. Wang, "Key technology for fully-mechanized top coal caving with large mining height in extra-thick coal seam," *Journal of China Coal Society*, vol. 38, no. 12, pp. 2089–2098, 2013.

[47] A. H. Wilson, "The stability of underground workings in the soft rocks of the coal measures," *International Journal of Mining Engineering*, vol. 1, no. 2, pp. 91–187, 1983.

[48] P. Konicek, K. Soucek, L. Stas, and R. Singh, "Long-hole destress blasting for rockburst control during deep underground coal mining," *International Journal of Rock Mechanics and Mining Sciences*, vol. 61, pp. 141–153, 2013.

[49] S. Yin, F. He, and G. Cheng, "Study of criterions and safety evaluation of rib spalling in fully mechanized top-coal caving face with large mining height," *Journal of China University of Mining and Technology*, vol. 44, no. 5, pp. 800–807, 2015.

[50] X. Fang, J. He, and H. Li, "A study of the rib fall mechanism in soft coal and its control at a full-mechanized top-coal caving face," *Journal of China University of Mining and Technology*, vol. 38, no. 5, pp. 640–644, 2009.

[51] L. Li, S. Zhang, J. Zhao, and C. Zhang, "Analysis and control of rib spalling of coal wall in isolated upward mining face," *Coal Engineering*, vol. 46, no. 7, pp. 81–84, 2014.

[52] J. Wan, "Mechanism of the rib spalling and the controlling in the very soft coal seam," *Journal of China Coal Society*, vol. 32, no. 8, pp. 785–788, 2007.

[53] Q. Yao, X. Li, B. Sun et al., "Numerical investigation of the effects of coal seam dip angle on coal wall stability," *International Journal of Rock Mechanics and Mining Sciences*, vol. 100, pp. 298–309, 2017.

[54] P. Yang, C. Liu, and F. Wu, "Breakage and falling of a high coal wall in a thick mined seam," *Journal of China University of Mining and Technolgoy*, vol. 42, no. 3, pp. 371–377, 2012.

[55] X. Du, J. Lu, K. Morsy, and S. Peng, "Coal pillar design formulae review and analysis," in *Proceedings of the 27th International Conference on Ground Control in Mining*, pp. 153–160, Morgantown, WV, USA, 2008.

[56] W. A. Hustrulid, "A review of coal pillar strength formulas," *Rock Mechanics*, vol. 8, no. 2, pp. 115–145, 1976.

[57] C. Mark, "The evolution of intelligent coal pillar design: 1981–2006," in *Proceedings of the 25th International Conference on Ground Control in Mining*, pp. 325–334, Morgantown, WV, USA, 2006.

[58] Z. Fang and J. P. Harrison, "Numerical analysis of progressive fracture and associated behaviour of mine pillars by use of a local degradation model," *Mining Technology*, vol. 111, no. 1, pp. 59–72, 2002.

[59] Z. Fang and J. P. Harrison, "Development of a local degradation approach to the modelling of brittle fracture in heterogeneous rocks," *International Journal of Rock Mechanics and Mining Sciences*, vol. 39, no. 4, pp. 443–457, 2002.

[60] J. W. Latilla, "Weak floors and their influence on pillar stability in Southern African collieries," in *Proceedings of SANIRE–The Miner's Guide through the Earth's Crust, South African National Institute of Rock Engineering*, pp. 71–78, Johannesburg, South African, 2004.

[61] M. M. Gadde, *Weak floor stability in the Illinois Basin underground coal mines, [Ph.D. thesis]*, West Virginia University, 2009.

[62] J. Lu, A. Ray, K. Morsy, and S. Peng, "Effects of rock/coal interface property on coal pillar strength," in *Proceedings of the 27th International Conference on Ground Control in Mining*, pp. 262–267, Morgantown, WV, USA, 2008.

[63] Y. Chen and S. Lu, *China Coal Mine Roadway Ground Control*, China University of Mining and Technology Press, Xuzhou, China, 1994.

[64] M. Salamon, "Modes of pillar and ribside failure–development and longwall," in *Strata Control for Coal Mine Design–Advanced Workshop*, pp. 1–40, Sydney, Australia, 1995.

[65] B. J. Madden, *An investigation into the factors affecting the strength of pillars in South African coal mines, [Ph.D. thesis]*, University of Witwatersrand, 1990.

[66] S. Chen, H. Zhou, W. Guo, H. Wang, and X. Sun, "Study on long-term stress and deformation characteristics of strip pillar," *Journal of Mining and Safety Engineering*, vol. 29, no. 3, pp. 376–380, 2012.

[67] Q. Bai, S. Tu, F. Wang, and C. Zhang, "Field and numerical investigations of gateroad system failure induced by hard roofs in a longwall top coal caving face," *International Journal of Coal Geology*, vol. 173, pp. 176–199, 2017.

[68] T. P. Medhurst and E. T. Brown, "A study of the mechanical behaviour of coal for pillar design," *International Journal of Rock Mechanics and Mining Sciences*, vol. 35, no. 8, pp. 1087–1105, 1998.

[69] M. Mathey, *Investigation into the mechanism of strength and failure in squat coal pillars in South Africa, [Ph.D. thesis]*, University of the Witwatersrand, 2016.

[70] G. Rashed and S. S. Peng, "Change of the mode of failure by interface friction and width-to-height ratio of coal specimens," *Journal of Rock Mechanics and Geotechnical Engineering*, vol. 7, no. 3, pp. 256–265, 2015.

[71] J. J. Muaka, S. Duma, P. Mushangwe et al., "Modelling hard rock jointed pillars using a distinct element and discrete fracture network approach considering the effect of a clay-filled shear structure," in *Proceedings of the 8th International Conference on Deep and High Stress Mining*, pp. 311–328, Perth, Australia, 2017.

[72] Y. Zhang, D. Stead, and D. Elmo, "Characterization of strength and damage of hard rock pillars using a synthetic rock mass method," *Computers and Geotechnics*, vol. 65, pp. 56–72, 2015.

[73] Y. Zhang and D. Stead, "Modelling 3D crack propagation in hard rock pillars using a synthetic rock mass approach," *International Journal of Rock Mechanics and Mining Sciences*, vol. 72, pp. 199–213, 2014.

[74] Y. Zhang, F. Ren, and X. Zhao, "Characterization of joint set effect on rock pillars using synthetic rock mass numerical method," *International Journal of Geomechanics*, vol. 17, no. 3, article 06016026, 2017.

[75] Y. Zhang and X. Zhao, "Characterisation of confinement effect on jointed rock pillars using a synthetic rock mass approach," *International Journal for Numerical and Analytical Methods in Geomechanics*, vol. 40, no. 12, pp. 1690–1711, 2016.

[76] N. Bahrani, P. K. Kaiser, and B. Valley, "Distinct element method simulation of an analogue for a highly interlocked, non-persistently jointed rockmass," *International Journal of Rock Mechanics and Mining Sciences*, vol. 71, pp. 117–130, 2014.

[77] B. Yu, Z. Zhang, T. Kuang, and J. Liu, "Stress changes and deformation monitoring of longwall coal pillars located in weak ground," *Rock Mechanics and Rock Engineering*, vol. 49, no. 8, pp. 3293–3305, 2016.

[78] H. Wang, Y. Jiang, Y. Zhao, J. Zhu, and S. Liu, "Numerical investigation of the dynamic mechanical state of a coal pillar during longwall mining panel extraction," *Rock Mechanics and Rock Engineering*, vol. 46, no. 5, pp. 1211–1221, 2013.

[79] T. D. Le, R. Mitra, J. Oh, and B. Hebblewhite, "A review of cavability evaluation in longwall top coal caving," *International Journal of Mining Science and Technology*, vol. 27, no. 6, pp. 907–915, 2017.

[80] R. Rafiee, M. Ataei, R. KhalooKakaie, S. E. Jalali, F. Sereshki, and M. Noroozi, "Numerical modeling of influence parameters in cavabililty of rock mass in block caving mines," *International Journal of Rock Mechanics and Mining Sciences*, vol. 105, pp. 22–27, 2018.

[81] A. Vakili and B. K. Hebblewhite, "A new cavability assessment criterion for longwall top coal caving," *International Journal of Rock Mechanics and Mining Sciences*, vol. 47, no. 8, pp. 1317–1329, 2010.

[82] J. Wang, B. Yu, H. Kang et al., "Key technologies and equipment for a fully mechanized top-coal caving operation with a large mining height at ultra-thick coal seams," *International Journal of Coal Science & Technology*, vol. 2, no. 2, pp. 97–161, 2015.

[83] H. M. Li, Y. Zhou, and X. X. Zhai, "The characteristics of top-coal deformation and smash with sub-level caving mining," *Journal of China Coal Society*, vol. 25, no. 4, pp. 352–355, 2000.

[84] Y. Zhang and J. Wu, "Crack-movement degree and caving characteristic of top-coal in longwall top coal caving mining," *Journal of China University of Mining and Technolgoy*, vol. 29, no. 5, pp. 506–509, 2000.

[85] X. Xie and T. Zhao, "Analysis on the top-coal caving structure of extra-thick hard coalseam with shallow depth in fully mechanized sublevel caving mining," *Journal of China Coal Society*, vol. 41, no. 2, pp. 359–366, 2016.

[86] S. Yan and J. Wu, "Analysis of top coal movement and damage characteristics in top-coal caving," *Chinese Journal of Rock Mechanics and Engineering*, vol. 15, no. 2, pp. 155–162, 1996.

[87] J. A. Nemcik, *Floor failure mechanisms at underground longwall face, [Ph.D. thesis]*, University of Wollongong, 2003.

[88] S. Aghababaei, G. Saeedi, and H. Jalalifar, "Risk analysis and prediction of floor failure mechanisms at longwall face in Parvadeh-I coal mine using rock engineering system (RES)," *Rock Mechanics and Rock Engineering*, vol. 49, no. 5, pp. 1889–1901, 2016.

[89] B. Indraratna, J. A. Nemcik, and W. J. Gale, "Review and interpretation of primary floor failure mechanism at a longwall coal mining face based on numerical analysis," *Géotechnique*, vol. 50, no. 5, pp. 547–557, 2000.

[90] P. Su and Z. Wei, "Depth of floor failure of stope with medium-thickness coal seam," *Geotechnical and Geological Engineering*, vol. 36, no. 2, pp. 1341–1347, 2018.

[91] J. A. Nemcik, B. Indraratna, and W. Gale, "Floor failure analysis at a longwall mining face based on the multiple sliding block model," *Geotechnical and Geological Engineering*, vol. 18, no. 3, pp. 175–192, 2000.

[92] J. Zhang, Y. Zhang, and T. Liu, *Rock Mass Permeability and Coal Mine Water Inrush*, Geological Publication House, Beijing, China, 1997.

[93] D. Healy, R. E. Rizzo, D. G. Cornwell et al., "FracPaQ: a MATLAB™ toolbox for the quantification of fracture patterns," *Journal of Structural Geology*, vol. 95, pp. 1–16, 2017.

[94] R. De La Vaissière, J. Morel, A. Noiret et al., "Excavation-induced fractures network surrounding tunnel: properties and evolution under loading," *Geological Society, London, Special Publications*, vol. 400, no. 1, pp. 279–291, 2014.

[95] S. Yin, F. He, G. Cheng, and Y. Zhao, "Study on asymmetric support of coal roadway nearby narrow pillar based on microcracks evolution process in fully-mechanized caving mining," *Journal of Mining & Safety Engineering*, vol. 33, no. 3, pp. 444–451, 2016.

[96] J. Wang, J. Jiang, G. Li, and H. Hu, "Exploration and numerical analysis of failure characteristic of coal pillar under great mining height longwall influence," *Geotechnical and Geological Engineering*, vol. 34, no. 2, pp. 689–702, 2016.

[97] H. Wu, N. Zhang, W. Wang, Y. Zhao, and P. Cao, "Characteristics of deformation and stress distribution of small coal pillars under leading abutment pressure," *International Journal of Mining Science and Technology*, vol. 25, no. 6, pp. 921–926, 2015.

[98] H. Zhang, Z. Wan, Z. Ma, and Y. Zhang, "Stability control of narrow coal pillars in gob-side entry driving for the LTCC with unstable overlying strata: a case study," *Arabian Journal of Geosciences*, vol. 11, no. 21, 2018.

[99] Y. Zhang, Z. J. Wan, F. C. Li et al., "Large deformation mechanism of roadway driving along goaf under unstable overlying rock stata," *Journal of Mining & Safety Engineering*, vol. 29, no. 4, pp. 451–458, 2012.

[100] H. Yin, L. Lefticariu, J. Wei et al., "A multi-method approach for estimating the failure depth of coal seam floor in a longwall coal mine in China," *Geotechnical and Geological Engineering*, vol. 34, no. 5, pp. 1267–1281, 2016.

[101] X. Lai, M. Cai, F. Ren, M. Xie, and T. Esaki, "Assessment of rock mass characteristics and the excavation disturbed zone in the Lingxin coal mine beneath the Xitian river, China," *International Journal of Rock Mechanics and Mining Sciences*, vol. 43, no. 4, pp. 572–581, 2006.

[102] H. Xie, Z. Chen, and J. Wang, "Fractal study on crack distribution in tunnels for sub-level caving mining," *Journal of China Coal Society*, vol. 22, no. 3, pp. 252–256, 1998.

[103] NR Council, *Rock Fractures and Fluid Flow: Contemporary Understanding and Applications*, National Academies Press, Beijing, China, 1996.

[104] Y. Liang, "Rock fracture skeleton tracing by image processing and quantitative analysis by geometry features," *Journal of Geophysics and Engineering*, vol. 13, no. 3, pp. 273–284, 2016.

[105] B. Slaker, E. Westman, J. Ellenberger, and M. Murphy, "Determination of volumetric changes at an underground stone mine: a photogrammetry case study," *International Journal of Mining Science and Technology*, vol. 26, no. 1, pp. 149–154, 2016.

[106] D. J. Benton, S. R. Iverson, L. A. Martin, J. C. Johnson, and M. J. Raffaldi, "Volumetric measurement of rock movement using photogrammetry," *International Journal of Mining Science and Technology*, vol. 26, no. 1, pp. 123–130, 2016.

[107] B. A. Slaker and K. M. Mohamed, "A practical application of photogrammetry to performing rib characterization measurements in an underground coal mine using a DSLR camera," *International Journal of Mining Science and Technology*, vol. 27, no. 1, pp. 83–90, 2017.

[108] T. Yang, Q. Yu, S. Chen, H. Liu, T. Yu, and L. Yang, "Rock mass structure digital recognition and hydro-mechanical parameters characterization of sandstone in Fangezhuang coal mine," *Chinese Journal of Rock Mechanics and Engineering*, vol. 28, no. 12, pp. 2482–2489, 2009.

[109] Q. Lei, J.-P. Latham, and C.-F. Tsang, "The use of discrete fracture networks for modelling coupled geomechanical and hydrological behaviour of fractured rocks," *Computers and Geotechnics*, vol. 85, pp. 151–176, 2017.

[110] W. S. Dershowitz and H. H. Einstein, "Characterizing rock joint geometry with joint system models," *Rock Mechanics and Rock Engineering*, vol. 21, no. 1, pp. 21–51, 1988.

[111] G. B. Baecher, "Statistical analysis of rock mass fracturing," *Journal of the International Association for Mathematical Geology*, vol. 15, no. 2, pp. 329–348, 1983.

[112] Y. Ju, C. Xi, Y. Zhang, L. Mao, F. Gao, and H. Xie, "Laboratory in situ CT observation of the evolution of 3D fracture networks in coal subjected to confining pressures and axial compressive loads: a novel approach," *Rock Mechanics and Rock Engineering*, vol. 51, no. 11, pp. 3361–3375, 2018.

[113] C. Wang, N. Zhang, Y. Han, Z. Xiong, and D. Qian, "Experiment research on overburden mining-induced fracture evolution and its fractal characteristics in ascending mining," *Arabian Journal of Geosciences*, vol. 8, no. 1, pp. 13–21, 2015.

[114] Q. Lei, J.-P. Latham, C.-F. Tsang, J. Xiang, and P. Lang, "A new approach to upscaling fracture network models while preserving geostatistical and geomechanical characteristics," *Journal of Geophysical Research: Solid Earth*, vol. 120, no. 7, pp. 4784–4807, 2015.

[115] E. Bonnet, O. Bour, N. E. Odling et al., "Scaling of fracture systems in geological media," *Reviews of Geophysics*, vol. 39, no. 3, pp. 347–383, 2001.

[116] D. P. Adhikary and H. Guo, "Measurement of longwall mining induced strata permeability," *Geotechnical and Geological Engineering*, vol. 32, no. 3, pp. 617–626, 2014.

[117] X. Song, M. Qian, and Z. Jin, "Study on the fragmental distributions regularity of top-coal fractured experiment for top-coal caving mining," *Journal of China Coal Society*, vol. 24, no. 3, pp. 261–265, 1999.

[118] J. Wang, X. Han, and P. Ren, "Identification of the damage state evolution in top coal caving mining," *Journal of China Coal Society*, vol. 41, no. S1, pp. 1–6, 2016.

[119] S. H. Prassetyo, R. Gamal, Y. Li, Y. Luo, and S. S. Peng, "The influence of interface friction and W/H ratio on the violence of coal specimen failure – a comparison between a bump and non–bump prone mines," in *30th International Conference on Ground Control in Mining*, pp. 162–168, Morgantown, WV, USA, 2011.

[120] Z. Zhang, R. Zhang, H. Xie, M. Gao, and J. Xie, "Mining-induced coal permeability change under different mining layouts," *Rock Mechanics and Rock Engineering*, vol. 49, no. 9, pp. 3753–3768, 2016.

[121] H. Xie, J. Xie, M. Gao et al., "Theoretical and experimental validation of mining-enhanced permeability for simultaneous exploitation of coal and gas," *Environmental Earth Sciences*, vol. 73, no. 10, pp. 5951–5962, 2015.

[122] R. Zhang, T. Ai, H. Li, Z. Zhang, and J. Liu, "3D reconstruction method and connectivity rules of fracture networks generated under different mining layouts," *International Journal of Mining Science and Technology*, vol. 23, no. 6, pp. 863–871, 2013.

[123] R. Zhang, T. Ai, H. W. Zhou, Y. Ju, and Z. T. Zhang, "Fractal and volume characteristics of 3D mining-induced fractures under typical mining layouts," *Environmental Earth Sciences*, vol. 73, no. 10, pp. 6069–6080, 2015.

[124] E. Hoek and E. T. Brown, "Practical estimates of rock mass strength," *International Journal of Rock Mechanics and Mining Sciences*, vol. 34, no. 8, pp. 1165–1186, 1997.

[125] E. Eberhardt, "Numerical modelling of three-dimension stress rotation ahead of an advancing tunnel face," *International Journal of Rock Mechanics and Mining Sciences*, vol. 38, no. 4, pp. 499–518, 2001.

[126] Q. Bai, *Mechanism and control on mining induced influences around longwall top coal caving face in extra seam with complex structures, [Ph.D. thesis]*, China University of Mining and Technology, 2015.

[127] T. Hong-Sheng, T. Shi-Hao, Z. Cun, Z. Lei, and Z. Xiao-Gang, "Characteristics of the roof behaviors and mine pressure manifestations during the mining of steep coal seam," *Archives of Mining Sciences*, vol. 62, no. 4, pp. 871–891, 2017.

[128] B. Ghabraie, G. Ren, and J. V. Smith, "Characterising the multi-seam subsidence due to varying mining configuration, insights from physical modelling," *International Journal of Rock Mechanics and Mining Sciences*, vol. 93, pp. 269–279, 2017.

[129] Z. Zhu, H. Zhang, J. Nemcik, T. Lan, J. Han, and Y. Chen, "Overburden movement characteristics of top-coal caving mining in multi-seam areas," *Quarterly Journal of Engineering Geology and Hydrogeology*, vol. 51, no. 2, pp. 276–286, 2018.

[130] L. Haifeng, Y. Baoyuan, and W. Lin, "Rock parameters inversion for estimating the maximum heights of two failure zones in overburden strata of a coal seam," *Mining Science and Technology*, vol. 21, no. 1, pp. 41–47, 2011.

[131] W. Guo, *Stability of coal wall and interaction mechanism with support in fully mechanized working face with great mining height, [Ph.D. thesis]*, China University of Mining and Technology, 2015.

[132] P. Gong, Y. Hu, Y. Zhao, and D. Yang, "Three-dimensional simulation study on law of deformation and breakage of coal floor on mining above aquifer," *Chinese Journal of Rock Mechanics and Engineering*, vol. 24, no. 23, pp. 4396–4402, 2005.

[133] S. C. Li, D. C. Wang, Q. Wang et al., "Development and application of large-scale geomechanical model test system for deep thick top coal roadway," *Chinese Journal of Rock Mechanics and Engineering*, vol. 38, no. 9, pp. 1522–1530, 2013.

[134] C. Wang, L. Wang, Z. Song, and L. Pan, "Testing study on 3D simulation material simulation for shallow coal seam mining," *Chinese Journal of Rock Mechanics and Engineering*, vol. 23, no. S2, pp. 4926–4929, 2004.

[135] H. Wang, Y. Wu, P. Cao, W. Zhang, and P. Xie, "Large scale loaded 3D-simualtion tests on mining steeply dipping seam," *Journal of China Coal Society*, vol. 40, no. 7, pp. 1505–1511, 2015.

[136] M. Ju, X. Li, Q. Yao, S. Liu, S. Liang, and X. Wang, "Effect of sand grain size on simulated mining-induced overburden failure in physical model tests," *Engineering Geology*, vol. 226, pp. 93–106, 2017.

[137] G. S. P. Singh and U. K. Singh, "A numerical modeling approach for assessment of progressive caving of strata and performance of hydraulic powered support in longwall workings," *Computers and Geotechnics*, vol. 36, no. 7, pp. 1142–1156, 2009.

[138] M. Shabanimashcool and C. C. Li, "Numerical modelling of longwall mining and stability analysis of the gates in a coal mine," *International Journal of Rock Mechanics and Mining Sciences*, vol. 51, pp. 24–34, 2012.

[139] N. E. Yasitli and B. Unver, "3D numerical modeling of longwall mining with top-coal caving," *International Journal of Rock Mechanics and Mining Sciences*, vol. 42, no. 2, pp. 219–235, 2005.

[140] T. D. Le, J. Oh, B. Hebblewhite, C. Zhang, and R. Mitra, "A discontinuum modelling approach for investigation of longwall top coal caving mechanisms," *International Journal of Rock Mechanics and Mining Sciences*, vol. 106, pp. 84–95, 2018.

[141] F. Gao, D. Stead, and J. Coggan, "Evaluation of coal longwall caving characteristics using an innovative UDEC Trigon approach," *Computers and Geotechnics*, vol. 55, pp. 448–460, 2014.

[142] C. Zhang, R. Mitra, J. Oh, I. Canbulat, and B. Hebblewhite, "Numerical analysis on mining-induced fracture development around river valleys," *International Journal of Mining, Reclamation and Environment*, vol. 32, no. 7, pp. 463–485, 2018.

[143] F. Gao, D. Stead, H. Kang, and Y. Wu, "Discrete element modelling of deformation and damage of a roadway driven along an unstable goaf — a case study," *International Journal of Coal Geology*, vol. 127, pp. 100–110, 2014.

[144] H. Xie, Z. Chen, and J. Wang, "Three-dimensional numerical analysis of deformation and failure during top coal caving," *International Journal of Rock Mechanics and Mining Sciences*, vol. 36, no. 5, pp. 651–658, 1999.

[145] I. Evans and C. Pomeroy, *The Strength, Fracture and Workability of Coal*, Pergamon Press, London, UK, 1966.

[146] S. E. Laubach, R. A. Marrett, J. E. Olson, and A. R. Scott, "Characteristics and origins of coal cleat: a review," *International Journal of Coal Geology*, vol. 35, no. 1-4, pp. 175–207, 1998.

[147] A. Lisjak, B. Tatone, O. Mahabadi, and G. Grasselli, "Block caving modelling using the Y-Geo hybrid finite-discrete element code," in *6th International Conference and Exhibition on Mass Mining (MassMin 2012)*, Sudbury, ON, Canada, 2012.

[148] A. Lisjak, O. K. Mahabadi, L. He et al., "Acceleration of a 2D/3D finite-discrete element code for geomechanical simulations using general purpose GPU computing," *Computers and Geotechnics*, vol. 100, pp. 84–96, 2018.

[149] D. Mas Ivars, M. E. Pierce, C. Darcel et al., "The synthetic rock mass approach for jointed rock mass modelling," *International Journal of Rock Mechanics and Mining Sciences*, vol. 48, no. 2, pp. 219–244, 2011.

[150] T. Medhurst, R. Rankine, and M. Kelly, "Development of a method for a longwall top coal caveability assessment," in *14th Coal Operators' Conference, University of Wollongong*, pp. 42–50, Wollongong, Australia, 2014.

[151] V. Palchik, "In situ study of intensity of weathering-induced fractures and methane emission to the atmosphere through these fractures," *Engineering Geology*, vol. 125, pp. 56–65, 2012.

[152] B. Nyberg, C. W. Nixon, and D. J. Sanderson, "NetworkGT: a GIS tool for geometric and topological analysis of two-dimensional fracture networks," *Geosphere*, vol. 14, no. 4, pp. 1618–1634, 2018.

[153] Y. Fadakar Alghalandis, "ADFNE: open source software for discrete fracture network engineering, two and three dimensional applications," *Computers & Geosciences*, vol. 102, pp. 1–11, 2017.

[154] R. Adams, "French thick seams mining practices," in *Symposium on Thick Seam Mining by Underground Methods*, pp. 41–50, Central Queensland, Australia, 1976.

[155] J. A. Wang and H. D. Park, "Coal mining above a confined aquifer," *International Journal of Rock Mechanics and Mining Sciences*, vol. 40, no. 4, pp. 537–551, 2003.

[156] J. Guo, G. Feng, P. Wang, T. Qi, X. Zhang, and Y. Yan, "Roof strata behavior and support resistance determination for ultra-thick longwall top coal caving panel: a case study of the Tashan coal mine," *Energies*, vol. 11, no. 5, p. 1041, 2018.